Check for updates

Earth and Space Science

RESEARCH ARTICLE
10.1029/2024EA003939

Post-Fire Sediment Yield From a Western Sierra Nevada Watershed Burned by the 2021 Caldor Fire

Amy E. East[1], Joshua B. Logan[1], Peter Dartnell[1], Helen W. Dow[1], Donald N. Lindsay[2], and David B. Cavagnaro[2]

[1]Pacific Coastal and Marine Science Center, U.S. Geological Survey, Santa Cruz, CA, USA, [2]California Geological Survey, Redding, CA, USA

Key Points:

- Sediment yield was quantified for 2 years after the 2021 Caldor Fire in a forested, heavily managed Sierra Nevada watershed
- Wetter-than-average conditions and intensive logging elevated second-year sediment yield to an order of magnitude above long-term values
- Reservoir surveys have useful applications in post-fire studies of 10^1- to 10^2-km^2 basins if the sedimentary signal-to-noise ratio is large

Supporting Information:

Supporting Information may be found in the online version of this article.

Correspondence to:

A. E. East,
aeast@usgs.gov

Citation:

East, A. E., Logan, J. B., Dartnell, P., Dow, H. W., Lindsay, D. N., & Cavagnaro, D. B. (2025). Post-fire sediment yield from a western Sierra Nevada watershed burned by the 2021 Caldor Fire. *Earth and Space Science*, *12*, e2024EA003939. https://doi.org/10.1029/2024EA003939

Received 23 AUG 2024
Accepted 2 DEC 2024

Author Contributions:

Conceptualization: Amy E. East
Data curation: Joshua B. Logan, Peter Dartnell, Donald N. Lindsay
Formal analysis: Amy E. East, Joshua B. Logan, Peter Dartnell, Helen W. Dow
Investigation: Amy E. East, Joshua B. Logan, Peter Dartnell, Helen W. Dow, Donald N. Lindsay, David B. Cavagnaro
Methodology: Joshua B. Logan, Peter Dartnell

Published 2025. This article is a U.S. Government work and is in the public domain in the USA. Earth and Space Science published by Wiley Periodicals LLC on behalf of American Geophysical Union.
This is an open access article under the terms of the Creative Commons Attribution-NonCommercial-NoDerivs License, which permits use and distribution in any medium, provided the original work is properly cited, the use is non-commercial and no modifications or adaptations are made.

Abstract Watershed sediment yield commonly increases after wildfire, often causing negative impacts to downstream infrastructure and water resources. Post-fire erosion is important to understand and quantify because it is increasingly placing water supplies, habitat, communities, and infrastructure at risk as fire regimes intensify in a warming climate. However, measurements of post-fire sediment mobilization are lacking from many regions. We measured sediment yield from a forested, heavily managed 25.4-km^2 watershed in the western Sierra Nevada, California, over 2 years following the 2021 Caldor Fire, by repeat mapping of a reservoir where sediment accumulated from terrain with moderate to high soil burn severity. Sediment yield was less than the geochronology-derived long-term average in the first year post-fire (conservatively estimated at 21.8–28.0 t/km^2), low enough to be difficult to measure with uncrewed airborne system (UAS) and bathymetric sonar survey methods that are most effective at detecting larger sedimentary signals. In the second year post-fire the sediment delivery was 1,560–2,010 t/km^2, an order of magnitude above long-term values, attributable to greater precipitation and intensive salvage logging. Hillslope erosion simulated by the Water Erosion Prediction Project (WEPP) model overestimated the measured amount by a factor of 90 in the first year and in the second year by a factor (1.9) that aligned with previously determined model performance in northern California. We encourage additional field studies, and validation of erosion models where feasible, to further expand the range of conditions informing post-fire hazard assessments and management decisions.

Plain Language Summary Watersheds typically produce more sediment after a wildfire because burned hillslopes erode easily, meaning that streams carry more sediment. Increased sediment delivery can cause problems for downstream infrastructure and water resources. Knowing how much sediment leaves a burned area is an important part of assessing risk to water supplies, infrastructure, and ecosystems, all of which are increasing concerns as climate change intensifies fire regimes, but measurements of sediment after wildfire are lacking from many regions. We studied these problems in a forested, heavily managed (logged) watershed in the western Sierra Nevada, California, over 2 years following the major Caldor Fire of 2021, by repeatedly mapping a reservoir where sediment accumulated from the burn zone. We detected only a small amount of sediment in the first year after the fire, but in the second year the sediment delivery was much larger due to more rain and logging activity that caused ground disturbances in the burned watershed. This study is part of a series documenting post-fire sedimentary processes in northern California, aiming to expand the knowledge base that resource managers can use in hazard assessments and decisions about managing water-storage reservoirs after a fire.

1. Introduction

Wildfire is a growing threat to communities, infrastructure, and ecosystems as climate continues to warm (Intergovernmental Panel on Climate Change, 2014; U.S. Global Change Research Program, 2023). As seasonally warmer, drier conditions decrease the moisture content in fuels, many regions are experiencing increases in fire-weather indices and intensified fire regimes (Jones et al., 2022; Rogers et al., 2020), including high-latitude forests and tundra (Feurdean et al., 2020; Kolden et al., 2024; Miner et al., 2022; Sierra-Hernández et al., 2022; Williams et al., 2020), the Mediterranean region (Morán-Ordóñez et al., 2020; Synolakis & Karagiannis, 2024; Turco et al., 2019; Vieira et al., 2023), Australia and New Zealand (Boer et al., 2020; Kemter et al., 2021; Melia et al., 2022), the Amazon River basin (Abatzoglou et al., 2019), and the western continental United States (e.g., Abatzoglou et al., 2019; Abatzoglou & Williams, 2016; Westerling & Bryant, 2008).

23335084, 2025, 1, Downloaded from https://agupubs.onlinelibrary.wiley.com/doi/10.1029/2024EA003939, Wiley Online Library on [23/01/2025]. See the Terms and Conditions (https://onlinelibrary.wiley.com/terms-and-conditions) on Wiley Online Library for rules of use; OA articles are governed by the applicable Creative Commons License

Resources: Donald N. Lindsay, David B. Cavagnaro
Supervision: Amy E. East
Validation: Joshua B. Logan, Peter Dartnell
Visualization: Joshua B. Logan, Helen W. Dow, David B. Cavagnaro
Writing – original draft: Amy E. East, Joshua B. Logan, Peter Dartnell, Helen W. Dow
Writing – review & editing: Amy E. East

As many studies have shown, wildfires alter soil properties, hydrologic characteristics, and sediment-transport processes. Soil changes and reduced vegetation commonly lead to streamflow, hillslope erosion, and sediment export all increasing after a fire (Chin et al., 2019, 2024; DeBano, 2000; Ebel & Moody, 2017; Ebel et al., 2022; Florsheim et al., 1991, 2017; Keller et al., 1997; Lane et al., 2006; Moody & Martin, 2009; Moody et al., 2013; Santi & Rengers, 2020; Shakesby & Doerr, 2006, and refer to the review of post-fire geomorphic effects by McGuire et al., 2024). If rainfall is sufficiently intense, runoff-generated post-fire debris flows form and can seriously endanger life, property, and infrastructure (e.g., Kean et al., 2011, 2019; Ouyang et al., 2023; Tang et al., 2019; Thomas et al., 2023). Even without debris flows, post-fire erosion can damage infrastructure downstream or downslope of burned terrain, can impact water quality, and may also reduce the storage capacity of reservoirs (Basso et al., 2021; Belongia et al., 2023; Elliott et al., 2024; Hallema et al., 2018; Jong-Levinger et al., 2024; Murphy et al., 2018, 2023; Nitzsche et al., 2024; Paul et al., 2022). The potential for major fires and post-fire erosion is greatest in settings that are neither fuel- nor flammability-limited (Littell et al., 2018), that is, places with enough moisture for dense vegetation to grow but dry enough seasonally to sustain large fires, and with high sediment availability and erosion from rain events. Most of the western United States (U.S.) meets these criteria (Goode et al., 2012; Noske et al., 2024), especially where topography is steep but not severely sediment-supply limited, underscoring the need for more place-based field and modeling studies of post-fire erosion there. Post-fire erosion is important to understand and quantify because it is increasingly placing water supplies, habitat, communities, and infrastructure at risk as fire regimes intensify in a warming climate.

Within the western U.S., California has had especially severe exposure to wildfire in recent decades, resulting in substantial life, property, and infrastructure loss and damage, as well as ecosystem disruption (e.g., Keeley & Syphard, 2016; Lancaster et al., 2021; MacDonald et al., 2023; Prein et al., 2022; Thorne et al., 2018; Wang et al., 2022; Western Forestry Leadership Coalition, 2022). Since the 1970s, warming has significantly increased the atmospheric vapor-pressure deficit in California, a climatic indicator of fuel dryness; as a result, the area burned annually has increased by a factor of five in that time (Williams et al., 2019). The greatest increase in burned area is evident since the mid-1990s (Turco et al., 2023) and is attributable especially to the rapid growth of large forest fires (Juang et al., 2022). Warmer, drier fire seasons have led to more frequent and intense extreme fires (Cunningham et al., 2024), with proportionally larger areas burning at high severity (Parks & Abatzoglou, 2020). Wildfire-related hazards, including those from post-fire sediment mobilization, are widely anticipated to continue increasing in California and around the western U.S. in the coming decades (Dow et al., 2024; East & Sankey, 2020; Goss et al., 2020; McGuire et al., 2024; Sankey et al., 2017; U.S. Global Change Research Program, 2023). Documenting and quantifying the rapidly shifting fire and post-fire landscape regime in this region is essential for effective resource protection and management now and in the future.

Many studies have established that sediment yield and erosion increase after fire (e.g., Cerdà & Lasanta, 2005; Cerdà et al., 1995; Moody & Martin, 2009), but the degree of increase varies widely with precipitation, slope, soil type, and soil burn severity, so granular place-based data are needed to constrain and predict future local-to-regional fire effects. This study evaluates physical landscape response after one of California's recent large forest fires, the 2021 Caldor Fire, to provide new data from an under-studied region and to increase resource managers' awareness of post-fire erosional responses in the western Sierra Nevada. We present the third in a series of case studies measuring post-fire erosion rates and sediment yield at 10^1- to 10^2-km^2 watershed scale for burned terrain in northern California, where post-fire measurements are sparse (cf. East et al., 2021, 2024).

Our approach uses repeat topographic and bathymetric sonar measurements of sediment surfaces in water-storage reservoirs to quantify sediment delivery from burned areas. Sediment deposits in reservoirs or natural lakes can provide valuable records of extreme events, land use, or more gradual hydroclimatic changes upstream (Conroy et al., 2008; Menounos & Clague, 2008; Smith et al., 2019; Snyder et al., 2006; Thurston et al., 2023), as long as sedimentation rates are high enough for event signals to be detectable above background "noise." Measuring post-fire sediment delivery using reservoir surveys avoids difficulties that commonly hinder other methods that, while valuable, have logistical disadvantages or do not resolve total post-fire sediment delivery. For example, fluvial suspended-sediment records resolve relative post-fire increases in sediment export (Jumps et al., 2022; Warrick & Rubin, 2007; Warrick et al., 2012) but miss the sediment moving as bed load, and in-stream sensors may be buried or destroyed if large flows occur. Hillslope erosion and downstream deposition can be measured using repeat lidar surveys (DeLong et al., 2018; Guilinger et al., 2020; Pelletier & Orem, 2014; Wicherski et al., 2017), typically applied over smaller focus areas (subaerially exposed surfaces at hillslope to small catchment scale). However, even bathymetric "green" lidar cannot be used to map in water deeper than light penetrates, limiting the scope of

23335084, 2025, 1, Downloaded from https://agupubs.onlinelibrary.wiley.com/doi/10.1029/2024EA003939, Wiley Online Library on [23/01/2025]. See the Terms and Conditions (https://onlinelibrary.wiley.com/terms-and-conditions) on Wiley Online Library for rules of use; OA articles are governed by the applicable Creative Commons License

lidar use in sediment-yield studies. Mapping reservoir deposits by other methods can yield useful data provided that the volume and aspect ratio of the reservoir, and management of the dam, allow sediment to be retained rather than rapidly transported downstream.

This investigation builds on previous related studies in California by measuring post-fire sediment yield in a new region and in a watershed with more complex pre- and post-fire forest management. East et al. (2021) measured sediment deposits after the 2018 Carr Fire in Whiskeytown Lake, in northern California's Klamath Mountains. The three watersheds included in that study (13, 24, and 29 km^2) had historical land use including dirt roads but had been relatively undisturbed since the land came under National Park Service management in the 1960s. Working in the upper Carmel River watershed (Santa Lucia Range, north-central California coast) after the 2016 Soberanes Fire, East et al. (2024) measured sediment yield from a 116-km^2 drainage area impounded by Los Padres Dam. That catchment had little anthropogenic land use, creating relatively simple, ideal conditions for a comparison of field results and output from the widely used Water Erosion Prediction Project (WEPP) model of post-fire erosion. In the present study we focus on a 25.4-km^2 burned watershed in the western Sierra Nevada (Figure 1). Unlike the two earlier case studies in this series, the watershed discussed herein had intensive pre- and post-fire logging activity. Our objective was to quantify sediment yield from the study catchment for 2 years post-fire. Although recognizing the difficulty of modeling a setting with such intensive, locally varying land use, we also applied the WEPP model to evaluate its performance in a more complex setting.

2. Study Area

The area of interest lies in the western foothills of the Sierra Nevada, in the transition zone between higher alpine terrain (climate type "Dsa," cold with dry, hot summers; Beck et al., 2023) and lower-elevation chaparral and grasslands of California's central valley ("Csa," temperate with dry, hot summers). The wet season, which occurs there from around November to April, has been shortening and sharpening as climate warms, with more intense rain occurring over a shorter season (Luković et al., 2021; Swain, 2021). The ecosystem in and around the study area is mid-montane conifer-dominated forest (fir and pine, with several oak species also). In the last two decades western Sierra Nevada forests have been hard-hit by drought and bark-beetle infestations, driving unprecedented tree mortality (Asner et al., 2015; Keeley & Syphard, 2016; Wang et al., 2022; Williams et al., 2019), and the associated dry fuel loading has contributed to recent large fires. Western-U.S. forest-fire area grew by 1,100% between 1984 and 2020, and some Sierra Nevada watersheds have seen even larger increases (Williams et al., 2022).

The Caldor Fire (Figure 1a) ignited in or near a campground in the Cosumnes River basin, El Dorado County, on 14 August 2021, amid record-breaking fire weather resulting from an intense heat dome over western North America (Jain et al., 2024). By the time of full containment on 21 October, the Caldor Fire had burned 898 km^2 in El Dorado, Alpine, and Amador Counties, destroying more than 1,000 structures (California Department of Forestry and Fire Protection [CalFire], 2023). This was only the second fire known to have crossed the crest of the Sierra Nevada, a few days after the Dixie Fire became the first to do so, 100 km to the north.

As the Caldor Fire advanced eastward, fueled by strong winds, it burned nearly the entire Sly Park Creek watershed above a reservoir, Jenkinson Lake (Figure 1b). Sly Park Creek drains a 25.4-km^2 watershed underlain by igneous (andesitic) and metasedimentary lithologies (Jennings et al., 2010) with maximum elevation 1,790 m above sea level, reaching the reservoir at 1,054 m. Most of the Sly Park Creek watershed burned at moderate and high soil burn severities in the Caldor Fire (Figure 1). Jenkinson Lake has retained water (and sediment) from Sly Park Creek and several other small watersheds (including water diverted through a tunnel from Camp Creek, immediately south of Sly Park Creek basin) since the two-part Sly Park Dam (58 m high) was completed in 1955, and has a design storage capacity of 50.6 million m^3 (Bureau of Reclamation, 2024). The reservoir, a drinking-water source managed by the El Dorado Irrigation District, suffered impaired water quality as a result of the fire (KCRA News, 2022).

Extensive tree harvesting occurred in the Sly Park Creek watershed before and after the Caldor Fire. Satellite imagery from June 2021, shortly before the fire, shows recently clear-cut areas, other less recently logged patches, and more mature forest areas, with dirt logging roads (Figure 2a). This type of logging mosaic is common for managed forests in the western Sierra Nevada and elsewhere. Lacking much vegetation cover, hillslopes logged before the fire were expected to erode during rain events even where burn severity was low to moderate (Figure 2b). In addition, after the fire, burned "hazard trees" were removed along a paved road (Mormon Emigrant

10.1029/2024EA003939

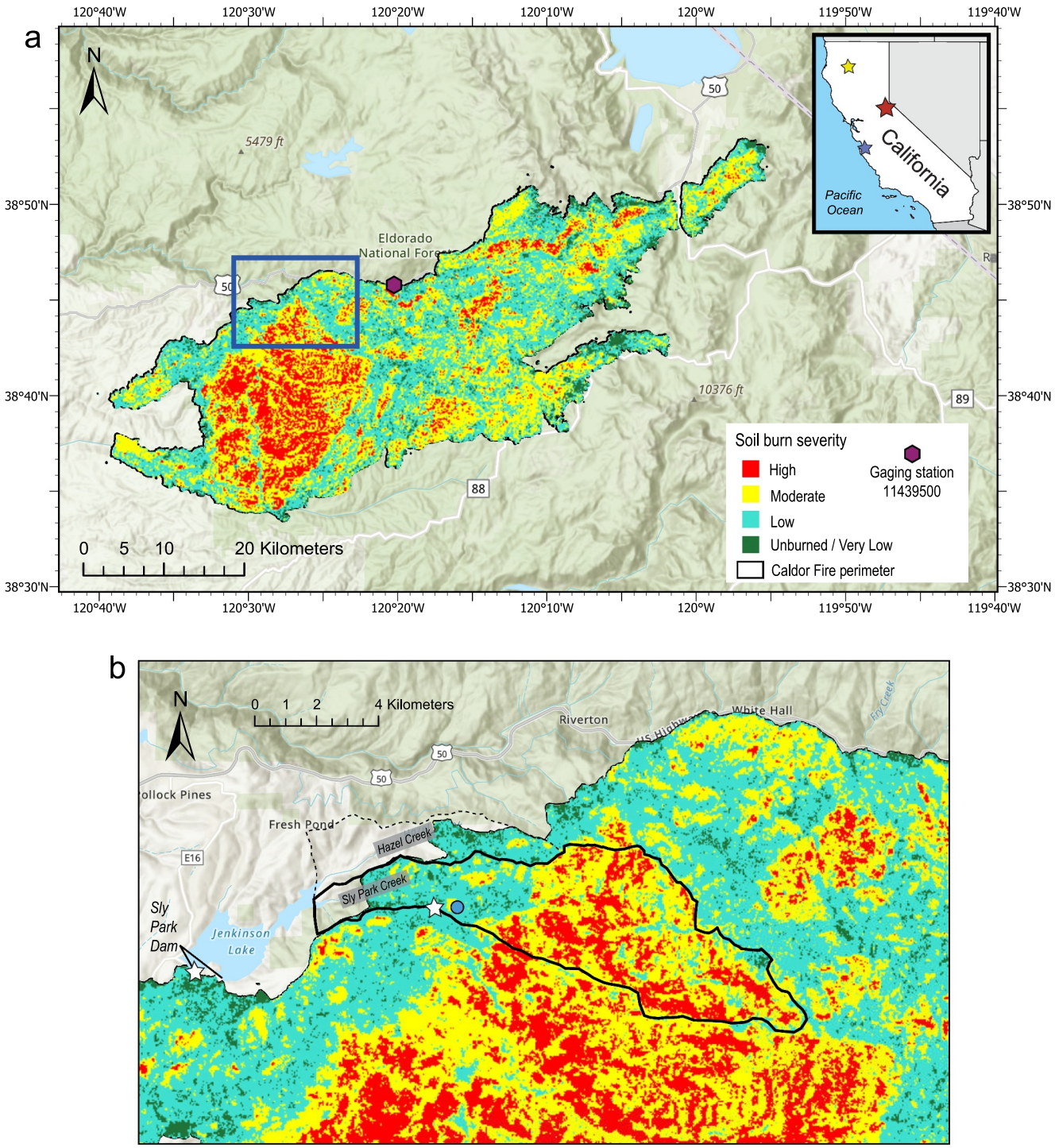


Figure 1. (a) Location map of the study area, showing the 2021 Caldor Fire burn zone. Color scheme indicates soil burn severity. Box indicates area shown in (b). On the inset map of California, red star shows this study location; smaller yellow and blue stars show area of sediment-yield studies after the Carr Fire (East et al., 2021) and Soberanes Fire (East et al., 2024), respectively. Purple point shows gaging station 11439500 on the South Fork American River near Kyburz (north of the fire perimeter at that location; U.S. Geological Survey, 2024a). (b) The Sly Park Creek watershed (outlined with solid black line), the primary focus of the study, and Hazel Creek (outlined with dashed black line), drain to the upper part of Jenkinson Lake. Blue circle indicates location of photographs shown in Figure 2. White stars indicate locations of two rain gages: one at Sly Park Dam, and one on the ridge bounding the south side of the watershed.

23335084, 2025, 1, Downloaded from https://agupubs.onlinelibrary.wiley.com/doi/10.1029/2024EA003939, Wiley Online Library on [23/01/2025]. See the Terms and Conditions (https://onlinelibrary.wiley.com/terms-and-conditions) on Wiley Online Library for rules of use; OA articles are governed by the applicable Creative Commons License

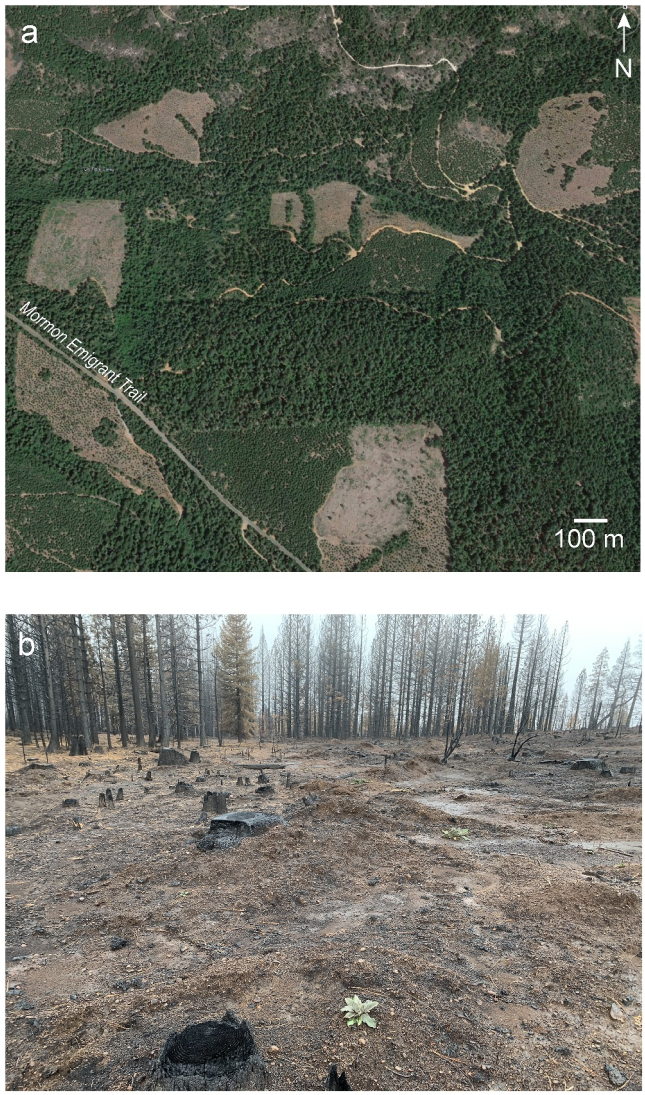


Figure 2. Photographs of logged forest areas within Sly Park Creek watershed. (a) Satellite image from 4 June 2021, before the Caldor Fire, showing evidence of pre-fire forest management: a mosaic of forest patches logged at different times, with dirt roads. Paved road (Mormon Emigrant Trail) is approximately the southern boundary of Sly Park Creek watershed. Image courtesy of Google Earth, Inc. (b) Photograph taken on 4 November 2021 in a part of Sly Park Creek watershed with moderate soil burn severity (refer to Figure 1b for location), several months after the Caldor Fire and approximately one week after the first post-fire storm activity. The foreground area had been logged before the fire. Poorly channelized overland-flow paths were observed in this burned, clear-cut area (foreground and right middle ground of image). Photo by USGS. Additional salvage logging of trees that were burned but not consumed by the fire would subsequently occur in Sly Park Creek watershed and along Mormon Emigrant Trail.

Trail; Figure 2a) on the south side of the watershed, and additional commercial salvage logging took place within the basin. Thus, human activities substantially affected land cover and watershed processes that contribute to erosion and sediment yield. Parsing the details of logging methods, time since clear cutting, dirt-road density and age, and other factors was beyond the scope of this study and these have been studied in detail by others (Keizer et al., 2018; Robichaud et al., 2010; Wagenbrenner et al., 2015, 2016). Instead, we viewed these land uses together as representative of many managed forests, and we considered the resulting sediment export (which we measured in Jenkinson Lake) to be an integrated signal of all upstream watershed processes and activities. We focus on overall sediment yield as the key parameter most needed by downstream water managers to understand local-to-regional fire consequences in a heavily managed forest setting.

Our study of post-fire sediment yield from Sly Park Creek spanned one average water year and one wet year. Streamflow is not measured directly on Sly Park Creek, but hydrologic conditions can be characterized using regional precipitation records and two local rain gages, one at Sly Park Dam and one on the watershed's southern boundary ridge (active beginning 7 June 2022; Lindsay, 2024). For additional hydrologic information we also referred to the nearest stream gage with long-term flow records and no immediate reservoir influence upstream: U.S. Geological Survey (USGS) gaging station 11439500, on the South Fork American River near Kyburz (the next major river basin north of the watersheds draining to Jenkinson Lake; Figure 1a). Average annual precipitation in the study area is 1,020–1,270 mm (Western Regional Climate Center, 2024). The first year post-fire, water year 2022 (1 October 2021–30 September 2022), saw 90–100% of normal precipitation during the wet season (National Oceanic and Atmospheric Administration, 2024). A rain gage at Sly Park Dam recorded 1,070 mm of rainfall in water year 2022 (Figure 3; California Department of Water Resources, 2022). The most intense rain occurred during an early season atmospheric-river storm on 24 and 25 October 2021, which delivered 236 mm of rain (22% of the water year total) and caused a 5-year flood on the nearby South Fork American River, calculated from the 15-min hydrograph at USGS gaging station 11439500 (Figure 1a; U.S. Geological Survey, 2024a). At Sly Park Dam that storm rainfall had a maximum 15-min intensity (I_{15}) of 24.4 mm/hr. Threshold rain intensities for post-fire debris flows vary geographically (McGuire & Youberg, 2020; Staley et al., 2013; Thomas et al., 2023); a median first-year I_{15} threshold of 37 mm/hr was assigned for stream segments in the Caldor Fire burn area, and some Sly Park Creek subbasins were considered to have high likelihood of post-fire debris flows (Staley et al., 2017; U.S. Geological Survey, 2024b). However, consistent with the actual rain intensities, no debris flows occurred in Sly Park Creek or its subbasins (based on close examination of aerial imagery).

The second year after the fire, water year 2023 (1 October 2022 to 30 September 2023) was much wetter, with wet-season precipitation 140%–150% of normal. The gage at the dam recorded 1,280 mm of rain from 1 October 2022 through 7 March 2023, but appeared to have malfunctioned thereafter (data past 7 March are not shown on Figure 3). A "family" of atmospheric rivers (Fish et al., 2019) occurring in close succession from 11 December to 16 January brought most of the rain in water year 2023. Four notable storms included a 30–31 December storm that delivered 253 mm of rain, with a maximum I_{15} of 20.3 mm/hr; another on 9–10 January (81 mm, maximum I_{15} 32.5 mm/hr); another over 13–16 January (181 mm, maximum I_{15} 16.3 mm/hr), and the final large event of the year on 3–4 March (112 mm, maximum I_{15} 20.3 mm/hr). The 30–31 December 2022 storm caused a 10-year flood at gaging station

23335084, 2025, 1, Downloaded from https://agupubs.onlinelibrary.wiley.com/doi/10.1029/2024EA003939, Wiley Online Library on [23/01/2025]. See the Terms and Conditions (https://onlinelibrary.wiley.com/terms-and-conditions) on Wiley Online Library for rules of use; OA articles are governed by the applicable Creative Commons License

10.1029/2024EA003939

23335084, 2025, 1, Downloaded from https://agupubs.onlinelibrary.wiley.com/doi/10.1029/2024EA003939, Wiley Online Library on [23/01/2025]. See the Terms and Conditions (https://onlinelibrary.wiley.com/terms-and-conditions) on Wiley Online Library for rules of use; OA articles are governed by the applicable Creative Commons License

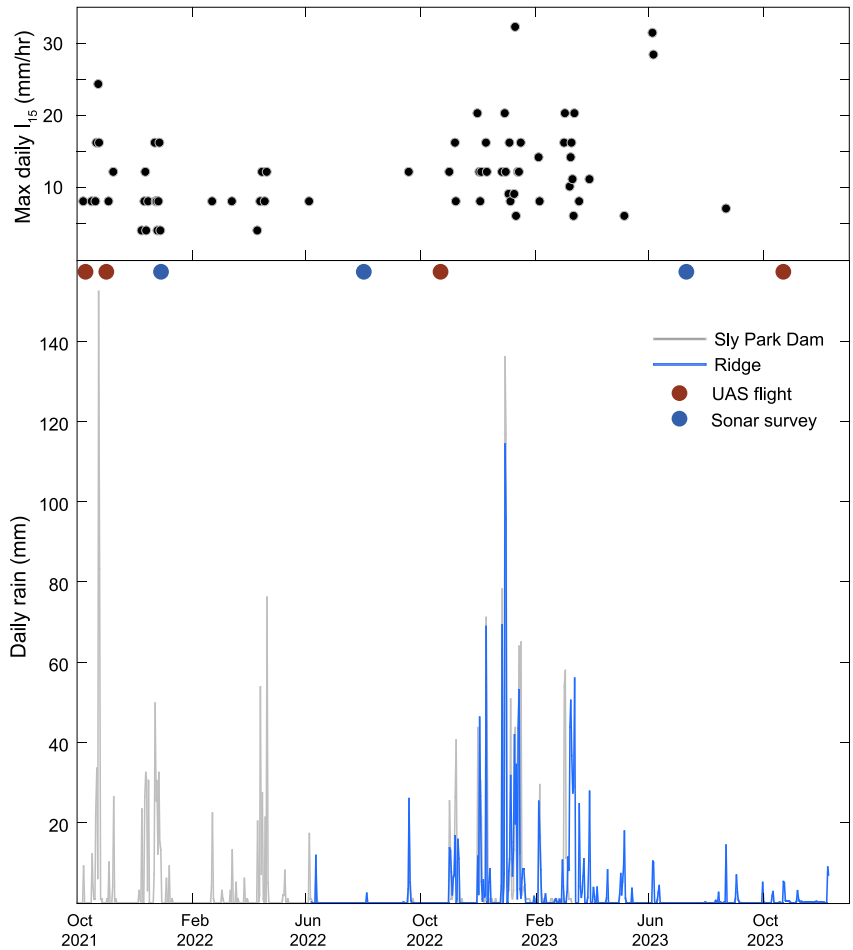


Figure 3. Daily rainfall (mm) measured at two gages (locations on Figure 1b): Sly Park Dam (gray line), at elevation 1,062 m, and on the ridge defining the southern boundary of Sly Park Creek watershed (blue line), at elevation 1,286 m. The rain gage on the ridge began collecting data on 7 June 2022. The gage at Sly Park Dam measures rainfall or rain-snow equivalent. The gage on the ridge has a tipping-bucket mechanism and sensor that only records during rain events and cannot sense snowfall. The gage at Sly Park Dam apparently malfunctioned after 7 March 2023 and its data after that are not shown. Upper plot shows maximum daily I_{15} values (in mm/hr) measured at either gage for days with substantial rainfall. Dates of topographic data collection by uncrewed airborne system (UAS) are shown with red circles; dates of bathymetric data collection by sonar survey are shown with blue circles.

11439500 (Figure 1a; U.S. Geological Survey, 2024a). Based on detailed examination of 1-m-pixel aerial and satellite imagery (discussed below) no areas of the Sly Park Creek watershed showed evidence of debris flows from 2022 or 2023 storms.

3. Methods

3.1. Field Data Collection

We estimated the post-fire sediment delivery to Jenkinson Lake by calculating changes between bathymetric and topographic digital elevation models (DEMs) collected in the first 2 years after the Caldor Fire. Due to the fluctuating water level in the reservoir during the study, both bathymetric and topographic surveys were required to fully resolve changes for the entire reservoir delta. The total area surveyed was 2.44 km^2. For additional information we also consulted Sentinel-2 satellite imagery of the study area.

Topographic surveys were conducted using uncrewed airborne systems (UAS) operated by the USGS on 13 October 2021, 4 November 2021, 25 October 2022, and 13 November 2023. The UAS surveys covered both the Hazel Creek and the Sly Park Creek inlet portions ("arms") of the reservoir delta (Figure 1b). The survey dates

23335084, 2025, 1, Downloaded from https://agupubs.onlinelibrary.wiley.com/doi/10.1029/2024EA003939, Wiley Online Library on [23/01/2025]. See the Terms and Conditions (https://onlinelibrary.wiley.com/terms-and-conditions) on Wiley Online Library for rules of use; OA articles are governed by the applicable Creative Commons License

were timed to bracket wet-season streamflow and coincided with low water levels to maximize data coverage on the subaerially exposed portion of the reservoir delta and shoreline. The 4 November 2021 survey was timed to document potential sediment input from the early season atmospheric river storm on 24–25 October 2021. That survey also served to re-establish the baseline condition of the delta for the interval until the next survey in fall 2022. The water level during the 13 November 2023 UAS survey was higher relative to the preceding UAS surveys, limiting the useable extent of the data from that survey to the Sly Park Creek inlet. The UAS surveys collected imagery for Structure-from-Motion (SfM) photogrammetry using a Ricoh GR II digital camera. Survey control was established using a network of approximately 20 ground control points (GCPs) with positions measured using real-time kinematic (RTK) global navigation satellite systems (GNSS) equipment. The RTK surveys were referenced to a benchmark established in the survey area for the duration of the study, with reference coordinates derived using the National Geodetic Survey Online Positioning User Service (NGS OPUS). We used SfM photogrammetric techniques in Agisoft Metashape 2.0 to derive DEMs, orthomosaic images, and topographic point clouds from the UAS imagery.

Bathymetric surveys of Jenkinson Lake including submerged portions of the reservoir delta were conducted on 11–12 January 2022, 16–17 August 2022, and 5–6 July 2023. These surveys used a SEA SWATHPlus 234-kHz interferometric bathymetric sidescan sonar system pole-mounted to the survey vessel (the 8-m-long USGS *R/V San Lorenzo*). An Applanix POS-MV (Position and Orientation System for Marine Vessels) with input from a differential global positioning system (DGPS) was used to position the vessel during data collection, and also to correct for vessel motion parameters (heave, pitch, and roll) during data post-processing. Sound-velocity profiles were collected throughout the survey days with a Castaway sound velocimeter and incorporated into data acquisition. Post-processed POS-MV Smoothed Best Estimate of Trajectory (SBET) files with input from NGS Continuously Operating Reference Station (CORS) base-station data were merged with the survey line files using BathySwath software and then the line files were imported into SonarWiz software. Soundings were cleaned of any obviously erroneous data points (e.g., artifacts arising from using sonar in shallow water) and gridded into 50-cm surfaces of the upper lake basin and delta. The base surfaces were exported as Erdas Imagine files in UTM zone 10, WGS84 coordinates vertically referenced to the WGS84 ellipsoid. The data were transformed to NAD83 horizontal coordinates using ArcGIS Pro ArcTool Command WGS_1984_(ITRF08)_To_NAD_1983_2011, and from ellipsoid heights to NAVD88 by applying a vertical transformation of +26.37 m (vertical uncertainty of 0.06 m), a value which was determined using the NOAA online VDATUM tool for a point in the upper reservoir basin. The NAVD88 bathymetric grids were then exported as geoTIFF files (Dartnell et al., 2024). The initial January 2022 bathymetric survey was used to establish the baseline post-fire condition of the submerged reservoir delta.

3.2. Calculations of Sediment Volume Change

Although the bathymetric surveys covered the entire reservoir, we observed no apparent sediment deposition in the lower lake (downstream of the immediate reservoir delta area) and thus limited our quantitative change analyses to the upper reservoir near the inlets of Hazel and Sly Park Creeks, the only part of Jenkinson Lake where vertical changes exceeded the detection limit for the survey methods. For deriving final volume and sediment-yield estimates, we limited our analysis areas to regions that exhibited change (based on close comparison of the DEMs).

Due to the varying water-surface elevations in Jenkinson Lake and non-concurrent timing of the topographic and bathymetric surveys, we grouped the DEMs to establish seasonal snapshots of the reservoir delta conditions bracketing each time-period of interest as follows: (a) the initial post-fire early season atmospheric river was bracketed by the October and November 2021 topographic UAS surveys. Bathymetry was not surveyed before the late-October 2021 storm, limiting that analysis interval to the subaerially exposed delta; (b) the first post-fire wet season of 2021–2022 was bracketed by the November 2021 and October 2022 topographic UAS surveys, and by the January 2022 and August 2022 bathymetric surveys; and (c) the second post-fire wet season of 2022–2023 was bracketed by the October 2022 and November 2023 topographic UAS surveys, and by the August 2022 and July 2023 bathymetric surveys.

When differencing the DEMs, due to differences in data-acquisition dates and methods, we did not merge the topographic and bathymetric data into continuous surfaces. We treated each DEM separately and derived DEMs-of-difference (DoD) for each combination of overlapping surfaces for a given time-period (UAS data differenced

23335084, 2025, 1, Downloaded from https://agupubs.onlinelibrary.wiley.com/doi/10.1029/2024EA003939, Wiley Online Library on [23/01/2025]. See the Terms and Conditions (https://onlinelibrary.wiley.com/terms-and-conditions) on Wiley Online Library for rules of use; OA articles are governed by the applicable Creative Commons License

from subsequent UAS data, UAS differenced from sonar bathymetry, and sonar bathymetry differenced from subsequent sonar bathymetry), and summed the volume-change values to derive overall estimates for the analysis area. For locations with spatial overlap between the data sets for a given time interval (i.e., UAS differenced from bathymetry, and bathymetry differenced from bathymetry), we preferentially used the UAS-differenced data due to the higher precision of SfM data over the subaerially exposed surfaces, compared to the lower precision of the bathymetric data, as artifacts are common in sonar data collected in shallow water. For small areas where data gaps exist in the DoD (resulting from no survey-to-survey overlap), we estimated volumetric change by interpolating from DoD values in the nearest adjacent locations. Our uncertainty analysis methods for each of these situations are discussed in detail below.

Several adjustments to the input DEMs were necessary prior to differencing. For the topographic (UAS SfM-generated) DEMs we adjusted for small horizontal differences (<1 m) observed between the October 2021 and November 2021 data sets relative to the two later data sets. These offsets were confined to the narrow Sly Park Creek arm of the reservoir delta and likely resulted from SfM alignment issues caused by the abundant overhead vegetation canopy in the narrow inlet, as well as decreased spatial precision of the RTK GNSS measurements of control-point locations in the narrow, vegetated corridor. To adjust for these offsets, we subdivided the topographic DEMs between the Sly Park Creek reservoir arm and the main delta. No horizontal offsets were observed in the main delta region, so those data were not adjusted. For the Sly Park Creek arm, we used the georeference tool in ESRI ArcGIS Pro to develop affine transformations to adjust the two 2021 data sets individually and improve horizontal alignment with the subsequent data sets. Using the orthomosaic image from October 2022 as a reference we identified 14 fixed, common, photo-identifiable objects visible in the 2021 orthomosaic images as tie points for deriving horizontal transformations, which we used to horizontally align the two 2021 Sly Park Creek DEMs with the October 2022 DEM. The resulting RMSE for each transformation was less than 8 cm, equivalent to less than one cell in the DEM rasters. These adjustments ensured accurate horizontal alignment between the surfaces prior to volume-differencing calculations.

We calculated volume changes by differencing the DEMs for each of the 3 time intervals of interest. The 2021 atmospheric-river storm preceded the first bathymetric survey, so DEM differencing for October–November 2021 was done using only UAS data of the subaerially exposed delta. We treated the main reservoir delta and Sly Park Creek arm separately and combined the respective volumes to derive total change estimates. For the Sly Park Creek arm, we vertically co-registered the two surfaces prior to differencing to correct for small (5–15 cm) non-uniform vertical differences present between the two data sets, assessed on stable objects such as small boulders and patches of visible bedrock common to both DEMs. As with the horizontal displacements, these vertical offsets likely resulted from effects of the narrow stream corridor and tree canopy on SfM image alignment and RTK precision. We used the vertical offsets on stable objects to develop an error-trend surface using the empirical Bayesian kriging tool in ESRI ArcGIS Pro and applied it to the initial DEM to produce a co-registered surface prior to differencing. Co-registration was not necessary for the DEMs in the main delta area, based on vertical agreement between the data sets in stable regions.

For the 2021–2022 interval we conducted DEM differencing for three separate combinations of surfaces: November 2021 UAS to October 2022 UAS, November 2021 UAS to August 2022 bathymetry, and January 2022 bathymetry to August 2022 bathymetry. For the UAS-to-UAS differencing, we performed vertical co-registration to the Sly Park Creek arm using the same procedure used for the previous time step. No co-registration was needed for the UAS-to-UAS differencing in the main reservoir delta. For the November 2021 UAS to August 2022 bathymetry differencing, we assessed vertical agreement between the data sets using large vertically stable regions on the exposed delta surface. These regions were subdivided into training and validation sets, with the latter withheld for subsequent use in estimating remaining vertical error in the final DoD. Using the mean vertical difference in four training regions, we applied a uniform vertical offset of 0.059 m to the UAS DEM prior to differencing. For the January 2022 bathymetry to August 2022 bathymetry differencing, we used a similar method to derive and apply a 0.076-m vertical adjustment to co-register the surfaces prior to differencing.

For the 2022–2023 interval we followed a similar differencing procedure to that used for 2021–2022. Within the Sly Park Creek arm, we co-registered the two surfaces using the same procedure used for the previous time steps. Owing to the higher water level during the 2023 UAS survey, no areas of overlap existed with the November 2022 UAS data set in the main delta area. Volume differences for the main delta region were thus calculated using the 2022 UAS data and 2022 bathymetry data, differenced against the 2023 bathymetry. Vertical agreement between

23335084, 2025, 1, Downloaded from https://agupubs.onlinelibrary.wiley.com/doi/10.1029/2024EA003939, Wiley Online Library on [23/01/2025]. See the Terms and Conditions (https://onlinelibrary.wiley.com/terms-and-conditions) on Wiley Online Library for rules of use; OA articles are governed by the applicable Creative Commons License

the surfaces was assessed using the same method described for the previous time steps, and we determined that no co-registration was necessary.

Uncertainty estimates for the volume calculations were derived using the methods of Anderson (2019). Vertical errors in DoDs were assessed using stable validation regions where no changes were observed. These regions were used to estimate random error, spatially correlated random error, and systematic error and these uncertainties were propagated for the total analysis area, reported at the 95% confidence level. To account conservatively for additional vertical errors observed in the bathymetric data outside of the analysis area, we increased the systematic error for volumes calculated from bathymetric change maps by doubling the mean vertical differences calculated in stable test regions. Similarly, to account conservatively for unknown vertical errors in the UAS data sets resulting from vegetation, shallow water in the stream channel (where resolving the sediment surface is difficult by SfM methods), and any other unknown errors, we increased the systematic error estimates for volumes calculated from UAS change maps by doubling the mean vertical differences calculated in stable test regions. Lastly, sufficiently large stable validation regions did not exist in the narrow, vegetated corridor of the Sly Park Creek arm. For that region we used the estimated vertical uncertainties from the main delta area but doubled these to account for possible remaining unknown errors not corrected by the vertical co-registration process used for those surfaces.

For each DEM differencing operation, we limited the areas used for volume calculations to the area of observed change, and we tabulated deposition and erosion volumes separately. In each time step we observed geomorphic changes consistent with reworking of the delta through fluvial processes when the reservoir water surface is low, for example, erosion of poorly consolidated bank sediment and mid-channel deposition along Sly Park Creek within the subaerially exposed portions of the delta deposit. To account for this and to avoid overestimating new sediment arrival, we report sediment yield in the Results section as the net volume change (deposition minus erosion) instead of reporting gross deposition.

3.3. Use of the WEPP Model

Because debris flows did not occur in the Sly Park Creek watershed following the Caldor Fire, we expanded the study scope opportunistically to also simulate post-fire erosion from this basin using the WEPP model, which can represent hillslope and channel erosion but not debris flows or other mass-wasting processes. This process-based model simulates hydrology of the surface and subsurface as well as hillslope and channel sediment mobilization and transport (Flanagan & Nearing, 1995; Flanagan et al., 2007; Laflen et al., 1991, 1997). WEPP was developed based on long-term field research into hydrologic and erosional processes and is now the most widely used post-fire hydrologic and sediment erosion model (Ebel et al., 2023; Lopes et al., 2021), being most commonly applied over plot to hillslope scale. Owing to the complex forest management before and after the fire in the Sly Park Creek watershed, we would not expect close agreement between the model and field estimates of sediment yield, as WEPP cannot closely represent the rapidly shifting forest cover. Therefore, this study should not be considered a true validation test of the WEPP model, as other studies have provided (Dobre et al., 2022; East et al., 2024; Robichaud et al., 2016). We simply provide WEPP results to accompany our field data expecting that resource managers in other similarly complex watersheds will need to apply some post-fire erosion model for predictive, management-driven purposes, and therefore would benefit from additional information regarding the performance of this commonly used model in a severely burned, heavily managed forest.

To model post-fire erosion in the study area we used WEPPcloud, the online WEPP interface released by Lew et al. (2022). This most recent version of WEPP utilizes soil and land-cover parameters, respectively, from the Natural Resources Conservation Service Soil Survey Geographic Database (NRCS SSURGO/STATSGO2; Reybold & TeSelle, 1989) and the USGS National Land Cover Database (NLCD; Jin et al., 2019). To factor in effects of the Caldor Fire we incorporated burn-severity coverage from the Monitoring Trends in Burn Severity (2024) database, which the model uses to modify soil and land-cover properties. To incorporate hydroclimate over the two water years after the fire we used the gridMET option in WEPPcloud, a 4-km gridded surface meteorological data set (Abatzoglou, 2013), having found in earlier work that WEPP run with gridMET reproduced field-measured sediment export more accurately than the Daymet alternative also available through WEPPcloud (Dow et al., 2024; East et al., 2024). WEPP uses daily variables from the gridded meteorological data sets together with monthly statistics from local weather stations to produce sub-daily storm characteristics using a synthetic storm generator, CLIGEN, resulting in simulated stream runoff that agrees well with actual streamflow

23335084, 2025, 1, Downloaded from https://agupubs.onlinelibrary.wiley.com/doi/10.1029/2024EA003939, Wiley Online Library on [23/01/2025]. See the Terms and Conditions (https://onlinelibrary.wiley.com/terms-and-conditions) on Wiley Online Library for rules of use; OA articles are governed by the applicable Creative Commons License

Table 1
Summary of Deposition, Erosion, and Net Volume Change Results for Jenkinson Lake Over the Time Intervals Investigated

Time interval	Total deposition detected (m^3)	Total erosion detected (m^3)	Net change (m^3)	Total uncertainty on net volume change (m^3)
October–November 2021	332	−15,400	**−15,100**	**±1,080**
2021–2022	4,260	−4,450	**−190**	**±1,220**
2022–2023	28,700	−994	**27,700**	**±2,130**

Note. Values are rounded to three significant figures. More spatially detailed and unrounded accounting of erosion and deposition is presented in Supporting Information S1 (Table S1).

magnitude and timing where measurements are available for comparison (e.g., Dobre et al., 2022; East et al., 2024). We also ran the model for water years 2022 and 2023 without including the soil burn severity coverage, to simulate sediment yield in the absence of the Caldor Fire. For each scenario we summed the daily sediment mass predictions to obtain total sediment mass produced in each of the two water years.

WEPPcloud generates sediment output for either hillslopes alone (based on rill and interrill erosion processes) or as sediment delivered to the chosen watershed outlet. This latter value is a combination of hillslope and channel erosion, but the values reflect only sediment transported to the outlet in one day, rather than truly aggregating the sediment that could be transported through channels to the basin outlet spending longer than a day in the channel. Therefore, although we report both output types below, hillslope-only values are expected to be more representative of erosion processes throughout the watershed. Each simulation was run for both Sly Park Creek (25.4 km^2), comprising most of the watershed area upstream of Jenkinson Lake, and the smaller Hazel Creek watershed (6.64 km^2) that was less affected by the Caldor Fire (~40% burned, mostly at low soil burn severity; Figure 1b). Additional details of the model input parameters are included in Supporting Information S1.

4. Results

4.1. Field-Based Estimates of Sediment Volume, Mass, and Yield

The topographic and bathymetric surveys detected geomorphic changes in Jenkinson Lake in each of the three time steps investigated (Table 1; Figures 4 and 5). All observed sediment deposition was confined to the Sly Park Creek arm of the reservoir and the upper portion of the reservoir delta, and almost all detected deposition occurred in the second water year after the Caldor Fire (2022–2023; Figures 4–6). As mentioned at the end of Section 3.2, to account for fluvial reworking of sediment in the upper reservoir delta when the lake surface is low, we report net volume changes instead of gross deposition (Table 1). This may under-count newly supplied sediment when the influx from upstream is smaller than the volume of delta sediment being eroded and reworked, and additional deposits presumably formed that were thin enough to be below the detection limits of our surveys (within the uncertainty range). Therefore, our estimates represent conservative calculations of post-fire deposition in the reservoir. A more detailed accounting of erosional and depositional areas is provided in Supporting Information S1 (Table S1).

Over the first water year following the Caldor Fire we did not detect substantial sediment deposition in the reservoir. In the first time step considered, October–November 2021, erosion in the upper reservoir deposits drove a net volume loss of 15,100 ± 1,080 m^3 (Table 1). We observed visually, and the UAS survey confirmed, channelized scour and new streambank collapse in both the Sly Park and Hazel Creek arms of the reservoir (red zones in Figure 4a). Some sediment presumably arrived in the subaqueous part of the reservoir unsurveyed over that time step, including the material newly remobilized from the upper reservoir deposit. However, this first storm appeared to be predominantly an erosional event on the reservoir delta. The subaerially exposed portions of the Sly Park Creek channel had a cobble-dominated gravel bed in the post-storm November 2021 survey, with no new sediment bars or other new depositional features. This contrasted notably with other post-fire settings where the first major storm often leaves streambeds oversupplied with fine sediment, causing widespread deposition and burying the previous channel features with sand and fine gravel as sediment supply temporarily overwhelms transport capacity (Chin et al., 2024; East et al., 2021; Florsheim & Chin, 2023; Thomas et al., 2023). During the remainder of that first water year, still no substantial deposition was detected. The net volume change for the second time step (ending in fall 2022) was within our uncertainty range, a loss of 196 ± 1,220 m^3. One distinctive depositional area was observed from that first post-fire winter: a sand-dominated, charcoal-bearing deposit of approximately 400 m^3

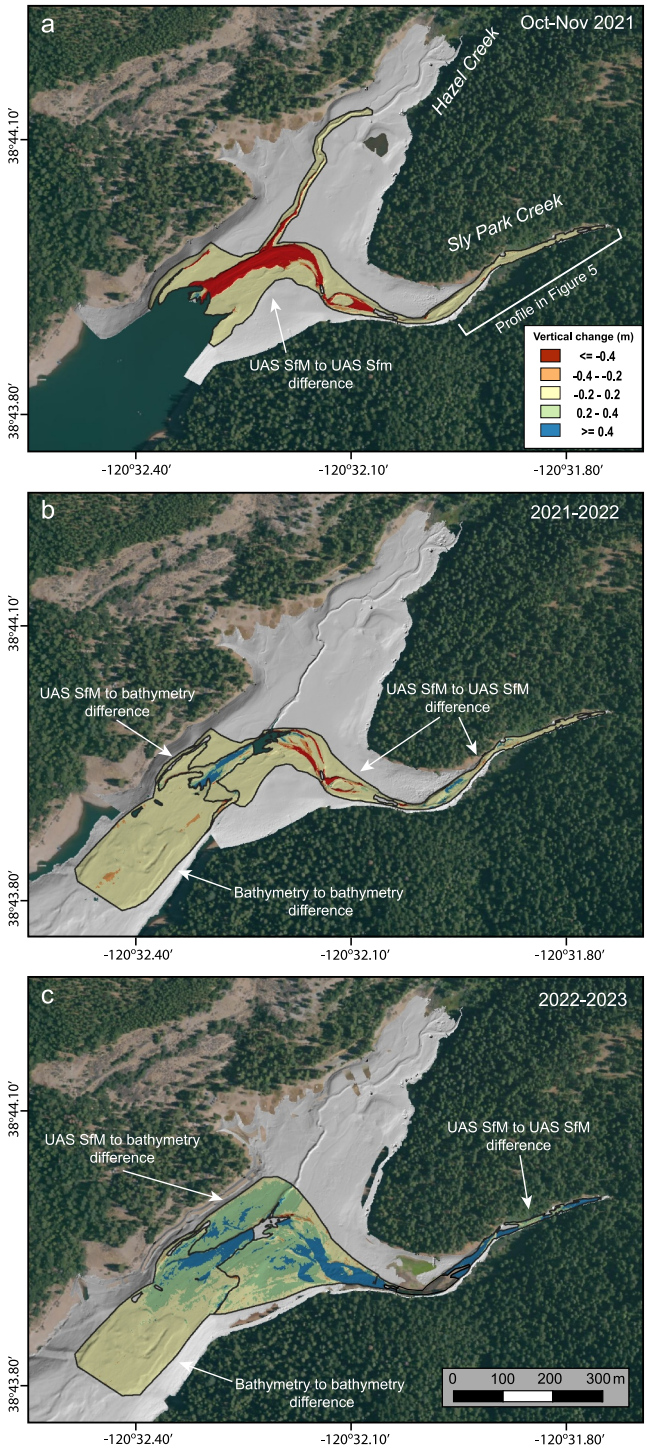


Figure 4. Results of geomorphic change analysis in the reservoir delta of Jenkinson Lake for 3 time intervals after the Caldor Fire: (a) October–November 2021; (b) 2021–2022, (c) 2022–2023. Refer to text for explanation of time steps. Color legend indicates vertical change detected from DEM differencing. Black polygons outline areas used for volumetric change analysis, identified by the data type used to create the DEM for that analysis area. Base image: U.S. Department of Agriculture, National Aerial Imagery Program (NAIP).

(395 ± 44 m^3) in the subaerially exposed Sly Park Creek channel (at 305–360 m along the profile shown in Figure 5; also Figure 6c). However, erosional losses from the upper reservoir exceeded the volume of that new deposit. Therefore, first-year post-fire sediment yield was essentially negligible (below our detection limit) if the estimate is based on net deposition throughout the entire surveyed area. However, if we consider the 400-m^3 sandbar in the Sly Park Creek reservoir arm to be the only unequivocally new sediment delivery that year, then, assuming a density range of 1,400–1,800 kg/m^3 (cf. Warrick et al., 2015), this equates to a mass of 550–710 t and a basin sediment yield of 21.8–28.0 t/km^2.

The second post-fire year saw considerably more sediment arriving in Jenkinson Lake (Figures 4–6). Our third time step, spanning 2022–2023 (water year 2023, a wet year), included net deposition of 27,700 ± 2,130 m^3 (Table 1). Using the same density assumptions as above, this volume represents a mass of 39,700–51,000 t, for a second-year basin sediment yield of 1,560–2,010 t/km^2. For these calculations we assume all detected sediment was produced by Sly Park Creek rather than Hazel Creek, as field evidence of new deposition was abundant in Sly Park Creek but we observed none in the Hazel Creek channel and reservoir arm (Figures 4–6). We also assume negligible sediment contribution from the Camp Creek Tunnel surface-water diversion. Although the tunnel operated during the 30–31 December 2022 storm (at flows of 1–17 m^3/s), it was then closed on 6 January and not reopened until 17 May, after the 2023 high-flow season finished (the tunnel was also closed during the October 2021 atmospheric-river storm). Within the Sly Park Creek reservoir arm, extensive new sandbars and mid-channel sand and gravel deposits were present in November 2023, locally exceeding 2 m thick and burying the preexisting cobble bed (Figures 5 and 6). The underlying cobbles were not yet re-exposed as of November 2023, indicating that sediment supply still exceeded transport capacity (cf. Florsheim & Chin, 2023). Macroscopic charcoal was visibly abundant in our field examination of sediment from those deposits. The final bathymetric survey in July 2023 also revealed widespread new deposition across the submerged portion of the reservoir delta (Figure 4). Subaqueous deposits accounted for 7,900 m^3 of the new sediment addition in that second year (28% of the net volumetric change; Supporting Information S1, Table S1).

4.2. WEPP Model Results

The WEPPcloud runs predicted greater post-fire sediment delivery than we measured in the field. For the first year after the Caldor Fire, the model predicted 56,753 t of hillslope sediment mobilization, the great majority from Sly Park Creek (56,064 t; Table 2), equivalent to modeled sediment yield for Sly Park Creek being 2,210 t/km^2. In contrast, the first-year sediment yield we inferred from field measurements was, at most, 21.8 to 28.0 t/km^2, indicating that the model overpredicted by a factor of ~90. In the second year post-fire, the modeled hillslope erosion mass was 88,756 t (87,248 t from Sly Park Creek), for a total sediment yield of 3,440 t/km^2. Compared to our field data, the model therefore overpredicted the second-year sediment yield from Sly Park Creek watershed (measured at 1,560–2,010 t/km^2) by a factor of 1.9. These values change little if we consider the model output for sediment delivered to the channel outlet, a value that incorporates channel erosion as well as hillslope but has no storage component, and therefore only includes eroded sediment that makes it to the outlet in a day. The modeled output for

23335084, 2025, 1, Downloaded from https://agupubs.onlinelibrary.wiley.com/doi/10.1029/2024EA003939, Wiley Online Library on [23/01/2025]. See the Terms and Conditions (https://onlinelibrary.wiley.com/terms-and-conditions) on Wiley Online Library for rules of use; OA articles are governed by the applicable Creative Commons License

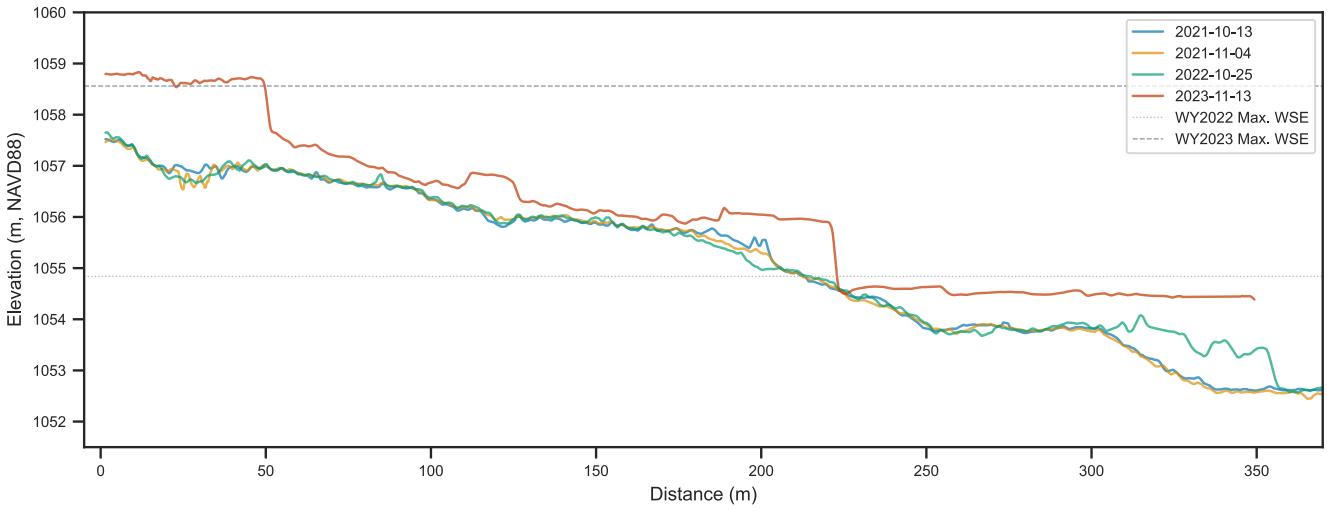


Figure 5. Profile through the upper Sly Park Creek arm of Jenkinson Lake, showing sediment surface elevations derived from UAS SfM-generated DEMs (distance "0 m" is the upstream limit of the streambed indicated on Figure 4c). Elevation is shown in reference to the NAVD88 datum. Maximum water-surface elevations (WSE) are shown for water years (WY) 2022 and 2023.

sediment delivered to the outlet cumulatively for Sly Park Creek in 2022 and 2023 was 54,681 and 82,114 t, respectively. The highest sediment yields tended to be from subcatchments in the upper watershed (Figure 7) where soil burn severity was greatest (predominantly moderate and high; Figure 1b).

Although overpredicting post-fire sediment mobilization, the WEPP model did accurately simulate much greater sediment supply from Sly Park Creek watershed compared to smaller and less-burned Hazel Creek (Table 2). The predictions of sediment mass in the burned scenarios for both years are, as expected, much higher than for the unburned scenarios, with the modeled burned values exceeding modeled unburned values by a factor of 79 for water year 2022 and a factor of 178 for water year 2023.

5. Discussion

This study provides findings needed to understand and anticipate post-fire landscape response in a heavily managed forest setting highly likely to see more large, intense fires in the coming decades. Wildfires in the study region are projected to continue responding strongly and nonlinearly to warming temperatures (MacDonald et al., 2023; Zhuang et al., 2021). Modeling by Gutierrez et al. (2021) showed a 19%–22% increase in fire risk for each 1°C of warming in the Sierra Nevada, indicating that summer burned area there could increase by 59 ± 33% by the 2040s. Future climate also will include greater magnitude and frequency of intense rain in this region (Allan & Soden, 2008; Huang et al., 2020; Swain et al., 2018; Trenberth, 2011), indicating that post-fire erosion will become a more common and intensified hazard (Kean & Staley, 2021; Oakley, 2021; Thomas et al., 2024). A recent statewide modeling analysis showed that post-fire erosion has indeed been increasing in California since the mid-1980s (Dow et al., 2024). Therefore, having additional place-based post-fire data from the western Sierra Nevada will assist resource managers to predict future local-to-regional fire effects in similar terrain and forest management situations.

The survey methods we used generate efficient coverage over large spatial scales and are designed to detect changes in surface elevations that exceed ~10–20 cm on submerged surfaces (for sonar bathymetry) and ~2–10 cm for subaerial SfM mapping. The advantage of these methods is to detect change at a scale relevant to surface-water storage facilities downstream of burned areas. For objectives requiring finer-scale examination of geomorphic changes and their causal processes, applying SfM or lidar to hillslopes and smaller catchments would be more suitable (e.g., Ellett et al., 2019; Guilinger et al., 2020, 2023; Rengers et al., 2021). The disadvantage of scaling up by using SfM and bathymetric sonar to detect changes in a reservoir is that these methods miss new sediment deposits that are thinner than the vertical detection limit and whose volume is smaller than our calculated uncertainty range. These methodological limitations, together with the lack of an October 2021 bathymetric survey (a complex field operation, logistically infeasible due to the rapid, early arrival of the first storm), likely

23335084, 2025, 1, Downloaded from https://agupubs.onlinelibrary.wiley.com/doi/10.1029/2024EA003939, Wiley Online Library on [23/01/2025]. See the Terms and Conditions (https://onlinelibrary.wiley.com/terms-and-conditions) on Wiley Online Library for rules of use; OA articles are governed by the applicable Creative Commons License

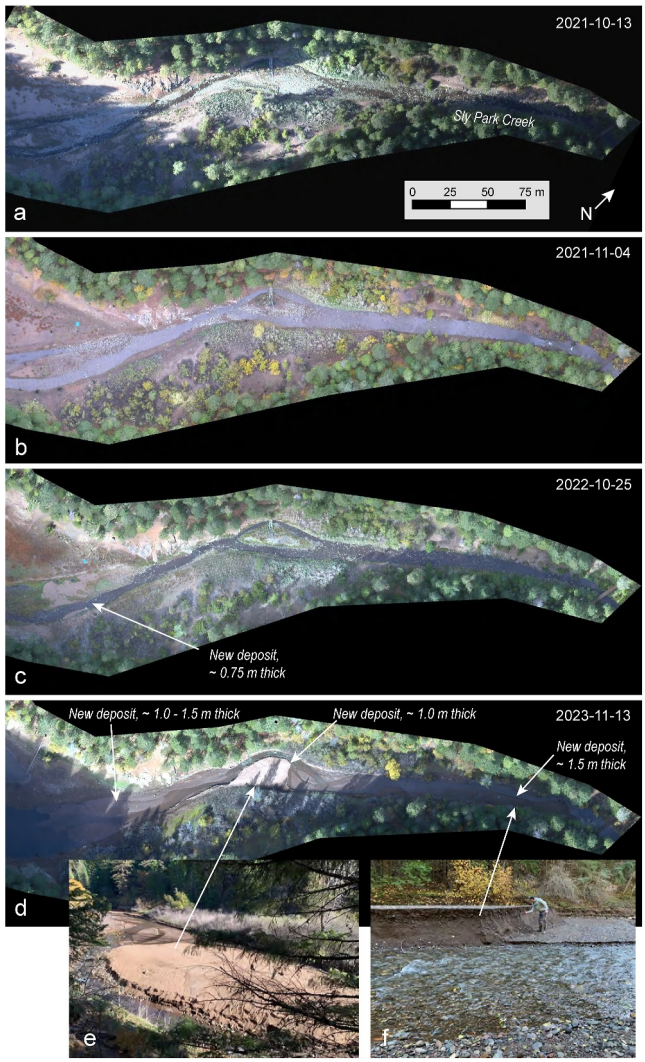


Figure 6. Imagery from the upper Sly Park Creek arm of Jenkinson Lake, showing changes in the sediment surface during the study period. (a) UAS orthoimage from 13 October 2021; (b) UAS orthoimage from 4 November 2021, showing essentially no change after the first post-fire storm; (c) UAS orthoimage from 25 October 2022, with arrow indicating the largest visible new sediment deposit (395 ± 44 m^3), which contained macroscopic charcoal; (d) UAS orthoimage from 13 November 2023, when new sand and gravel deposits covered the previous channel bed and buried geomorphic features (refer to Figure 5 also); (e) oblique field photo taken 13 November 2023 showing a large sandbar approximately 1 m thick, spanning nearly the full width of the reservoir arm; (f) oblique field photo showing 1.5-m-thick new sand and gravel deposit near the upstream end of the reservoir, with the sediment deposit at person's shoulder level being approximately the 2023 maximum water surface elevation (photos: A. East).

caused us to under-count first-year sediment influx to Jenkinson Lake. A water-treatment plant immediately below Sly Park Dam required mitigation of high turbidity in 2021 and 2022 from a combination of ash and suspended sediment, indicating that some fine material from the burned area passed through the lake without settling. Turbid plumes appear in several satellite images, too (Figure 8). It is also likely that some of the sediment mobilized from hillslopes in the first year post-fire had not moved all the way downstream to the reservoir that year, but was stored in channels until the second, wetter year provided more fluvial transport capacity (cf. Guilinger et al., 2023). We note also that aspiring to detect change using sedimentary deposits downstream from disturbed areas assumes that the mobile sediment supply remains sufficient to generate detectable signals, rather than being severely limited by low rates of production from bedrock or already exhausted by prior disturbances (e.g., Ryan et al., 2024). The soil-mantled hillslopes in the study watershed are not thought to be strongly supply limited.

Our calculations indicate that sediment delivery after the Caldor Fire did not compromise water storage significantly in Jenkinson Lake. The net sediment volume gain of 27,700 m^3 represented only 0.06% of the 50 million m^3 design capacity of the reservoir. Therefore, despite the water-quality impacts, and unlike some other California reservoirs that have lost large proportions of storage space to post-fire sedimentation (East et al., 2024; Los Angeles County, 2021, 2023), storage space in this reservoir was essentially unaffected, owing to low first-year sediment runoff and the relatively large reservoir volume. Given that most post-fire erosion in California occurs upstream from reservoirs (Dow et al., 2024), and that water-supply infrastructure can be damaged by relatively small increases in sediment loading (Jong-Levinger et al., 2022, 2024), post-fire erosion nevertheless remains a growing concern for western U.S. water management (Murphy et al., 2018; Randle et al., 2021; Sankey et al., 2017). These effects will be felt most by communities utilizing small reservoirs, where temporarily higher sedimentation rates can eliminate a relatively larger proportion of storage capacity.

The sediment-yield estimate of 1,560–2,010 t/km^2 for the second post-fire year is approximately one order of magnitude greater than the regional rate derived from cosmogenic nuclide geochronology. No published erosion rates exist for the Cosumnes River basin, but a collection of millennial-scale ^{10}Be-based catchment-averaged erosion rates at a similar position between the mountain front and the crest in the southern Sierra Nevada show a mean erosion rate of 0.04 mm/yr (Callahan et al., 2019). Additionally, analysis of ^{26}Al/^{10}Be ratios in fluvial sediment in a cave above the Stanislaus River (70 km south of the Cosumnes River and two major drainages away from our study area) suggests an average erosion rate of 0.06 mm/yr over the last 1.6 Ma (Stock et al., 2005). Other measurements of erosion in the Sierra Nevada are from locations much farther away and/or dissimilar to our study area (e.g., glacial uplands or deeply incised canyons). Combined, the available rates suggest an average denudation rate of 0.05 mm/yr, which is equivalent to a sediment yield of 133 t/km^2/yr, less than a tenth of our estimated second-year post-fire yield. This relative increase after fire is in line with other studies in the literature—although post-fire yields may range from 1.2 to 1,600 times above pre-fire values, an increase of one to two orders of magnitude is commonly reported (refer to review by McGuire et al., 2024). Some of the higher values in published studies were influenced by post-fire debris flows, though, complicating comparison with our results. The sediment yield we estimated for Sly Park Creek in 2022–2023 (water year 2023), a year without debris flows and 140%–150% of normal rain, was similar to values from two of three forested (but not recently logged) watersheds studied after the Carr Fire in the eastern Klamath Mountains (2,700 and 4,100 t/km^2/yr), also

23335084, 2025, 1, Downloaded from https://agupubs.onlinelibrary.wiley.com/doi/10.1029/2024EA003939, Wiley Online Library on [23/01/2025]. See the Terms and Conditions (https://onlinelibrary.wiley.com/terms-and-conditions) on Wiley Online Library for rules of use; OA articles are governed by the applicable Creative Commons License

23335084, 2025, 1, Downloaded from https://agupubs.onlinelibrary.wiley.com/doi/10.1029/2024EA003939, Wiley Online Library on [23/01/2025]. See the Terms and Conditions (https://onlinelibrary.wiley.com/terms-and-conditions) on Wiley Online Library for rules of use; OA articles are governed by the applicable Creative Commons License

Table 2
Results of WEPP Model Simulations of Sediment Mass and Yield Due To Hillslope Erosion for Burned and Unburned Scenarios in Sly Park and Hazel Creeks in Water Years 2022 and 2023

	Water year 2022		Water year 2023	
WEPP scenario	Mass (t)	Yield (t/km^2)	Mass (t)	Yield (t/km^2)
Sly Park Creek, burned	56,064	2,210	87,248	3,440
Sly Park Creek, unburned	583	23.0	333	13.1
Hazel Creek, burned	689	104	1,508	227
Hazel Creek, unburned	134	20.2	165	24.9
Estimates from field measurements	550–710	21.8–28.0	39,700–51,000	1,560–2,010

Note. Results from Hazel Creek do not reflect solely "post-fire" sediment yield, as only ~40% of that watershed burned. Drainage area is 25.4 km^2 for Sly Park Creek and 6.64 km^2 for Hazel Creek. Values based on field measurements are shown in lowest row for comparison (refer to text for details).

measured in a wet year (133% of normal rain, without debris flows; East et al., 2021) and greater than in a Coast Range watershed where unlogged forested and chaparral hillslopes burned at moderate and low severity (854–1,100 t/km^2/yr with major flooding and ~300% of normal rain, but no post-fire debris flows; East et al., 2024).

The sediment yield being so much greater in the second year of our study than in the first year is attributable to the much wetter winter in water year 2023 (precipitation being a major factor in post-fire erosion magnitude, e.g., Cole et al., 2021; Dow et al., 2024; Miller et al., 2011) and also to the effects of intensive salvage logging. For the purpose of this study these influences are not separable. Our findings are intended to represent the combined result downstream, quantifying the end product from a severely burned basin being managed in much the same way as many other watersheds in the Sierra Nevada. Based on examination of satellite imagery and public records, 23.5% of the Sly Park Creek watershed was newly logged between spring 2022 and summer 2023 (Figures 8 and 9), on top of 11.1% of the basin clear-cut recently before the Caldor Fire. Following California Forest Practice Rules (California Board of Forestry and Fire Protection, 2024), this commercial salvage logging included clear-cutting, ground-based yarding to extract the cut timber, and applying herbicide to limit regrowth of non-commercial vegetation. Ground-based yarding practices, which include the use of heavy equipment such as feller-bunchers, skidders, tractors, forwarders, or processors to cut and extract the timber, and skid-trail construction, are well known to increase sediment yield from burned (and unburned) ground (Ramos-Scharrón & LaFevor, 2018; Robichaud et al., 2010; Wagenbrenner et al., 2016, 2023). The standard practices applied in Sly Park Creek did not appear to include leaving slash or mulch on the ground to reduce erosion

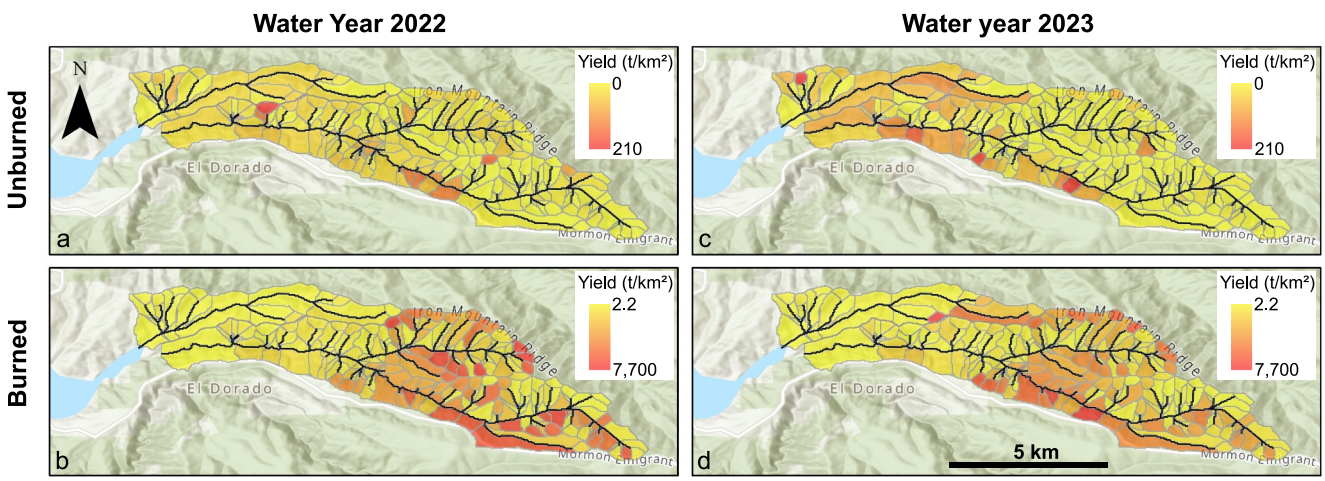


Figure 7. Results of WEPP model analysis of hillslope sediment yield produced in Sly Park Creek and Hazel Creek for water years 2022 (a, b) and 2023 (c, d). Model runs for the unburned scenario in (a) and (c) omitted the Caldor Fire soil burn severity map that was used in the burned scenario (b, d). Greater values in the eastern, upstream region of Sly Park Creek watershed reflect greater soil burn severity there (compare with Figure 1b). Refer to Figure S1 in Supporting Information S1 for erosion values presented in units of mass.

10.1029/2024EA003939

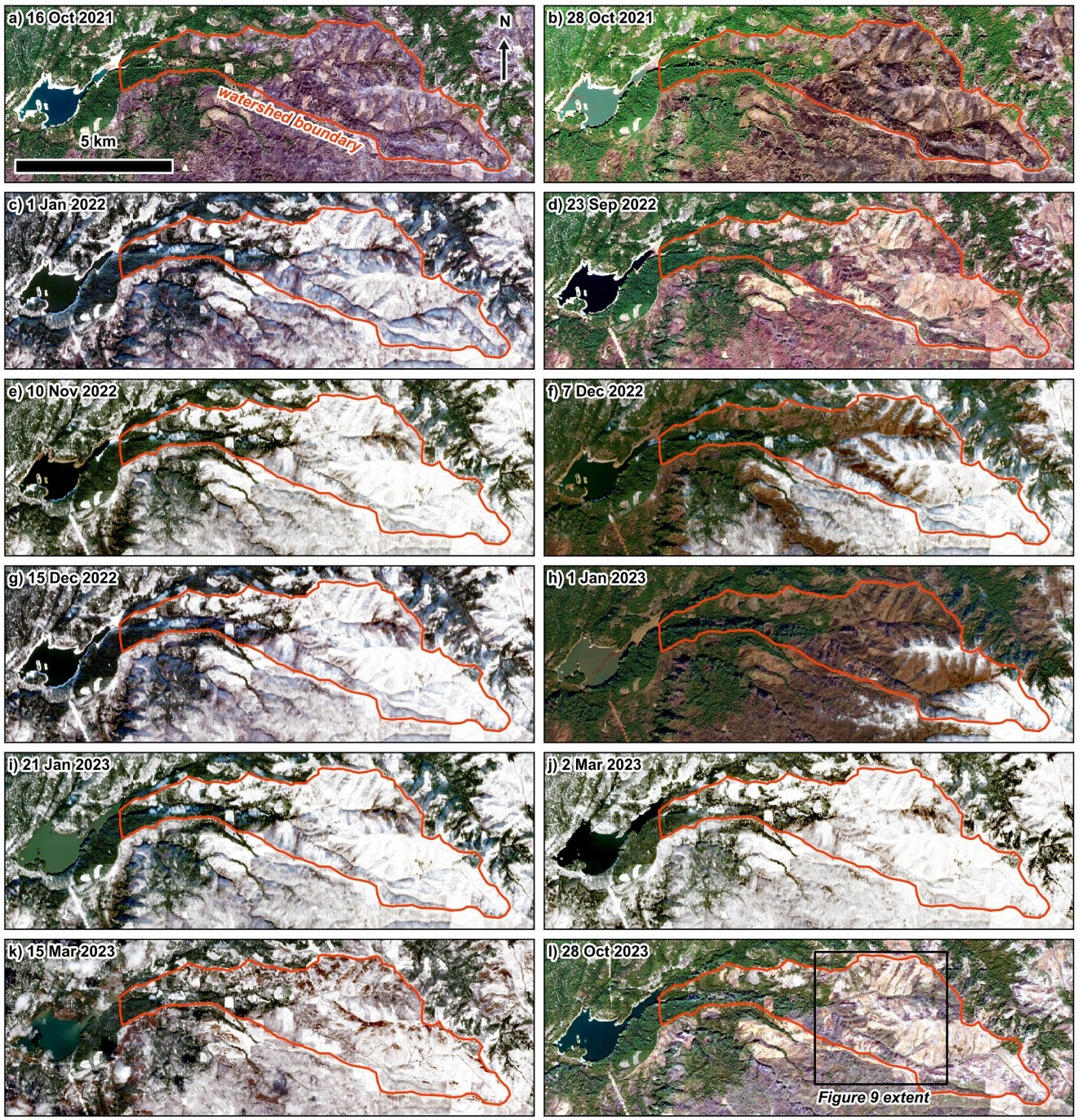


Figure 8. Satellite images (Sentinel-2) showing Jenkinson Lake and the Sly Park Creek watershed (outlined in red) for multiple dates after the Caldor Fire: (a) 16 October 2021; (b) 28 October 2021; (c) 1 January 2022; (d) 23 September 2022; (e) 10 November 2022; (f) 7 December 2022; (g) 15 December 2022; (h) 1 January 2023; (i) 21 January 2023; (j) 2 March 2023; (k) 15 March 2023; and (l) 28 October 2023. Effects of salvage logging are evident by comparing panels (a), (d), and (l); refer also to Figure 9. As discussed in the text, these images also demonstrate that the snow line shifts through the elevation of the study area repeatedly during a winter season. Turbid plumes are visible in the lake in (h), on 1 January 2023, and (k), on 15 March 2023, following winter storms.

(Jonas et al., 2019; Keizer et al., 2018; Prats et al., 2021) or installing erosion barriers (except immediately upslope of protected water courses, e.g., Robichaud et al., 2019). However, the harvesting activities concluded by contouring dirt roads ("contour ripping") on some slopes to promote infiltration, providing some erosion mitigation. Comparing our measured 2022–2023 sediment yield to other post-fire data from salvage-logged areas in this region, our values were an order of magnitude above those that Olsen et al. (2021) reported

23335084, 2025, 1, Downloaded from https://agupubs.onlinelibrary.wiley.com/doi/10.1029/2024EA003939, Wiley Online Library on [23/01/2025]. See the Terms and Conditions (https://onlinelibrary.wiley.com/terms-and-conditions) on Wiley Online Library for rules of use; OA articles are governed by the applicable Creative Commons License

10.1029/2024EA003939

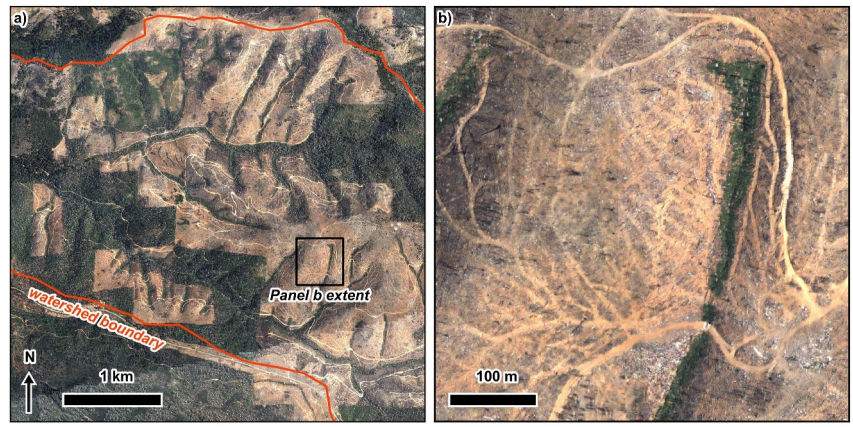


Figure 9. Orthomosaic image within eastern Sly Park Creek watershed on 22 May 2024 (location on Figure 8l), showing effects of post-fire forest management operations including clear-cut salvage logging and new skid trails and roads. Panel (b) shows a close-up view of the boxed area in (a). Image courtesy of the Fire Integrated Real-Time Intelligence System Program (FIRIS), California Office of Emergency Services (2024).

after the 2013 Rim Fire in the Sierra Nevada (110–320 t/km^2); our results were comparable to the high end of sediment yields reported by Cole et al. (2021) for salvage-logged plots after the 2015 Valley Fire, where mean annual sediment yield was 640 t/km^2/yr but values ranged up to 2,550 t/km^2/yr.

The bare-ground appearance of much of Sly Park Creek watershed by the end of our study, with no substantial vegetation recovery and signs of mechanical ground disturbance still clearly visible (Figure 9), implies that sediment yield will not approach pre-fire, pre-harvest conditions for years to possibly a decade (cf. Kinoshita & Hogue, 2011; Vieira et al., 2016). Post-fire hydrologic recovery is slower for forests than for other vegetation types, lasting an average of 6 years in the western U.S., because forests have a larger capacity for rain interception and use more water through transpiration (Williams et al., 2022); hydrologic recovery will be linked closely to future erosion and sediment yield. It is also likely that sediment that eroded from hillslopes in the first 2 years after the fire and was still stored in channels above the reservoir at the time of our final data collection will move downstream in future wet seasons (cf. Florsheim et al., 2017). The overall time scale for sediment yield to recover from the coupled disturbances of fire and post-fire forest management will depend on future water availability, especially stream runoff, and hillslope sediment supply (Ryan et al., 2024).

Finally, we note that the post-fire erosion predicted by WEPP exceeded the amount measured using sediment accumulation in the reservoir. Expecting close agreement between field and model results at 25-km^2 watershed scale would be unrealistic in view of the complex disturbances of salvage logging, but the mere occurrence of those disturbances suggested that a model would underestimate rather than overestimate sediment mobilization. The difference between WEPP results and our field values (the model overestimating by factors of 90 and 1.9 for the first and second years, respectively) is too large to be attributed to our surveys' detection limits. Some of the overestimation, especially in the first year, may reflect sediment that had mobilized from hillslopes but not yet moved downstream all the way to the reservoir (Wagenbrenner & Robichaud, 2014). Little aggradation was apparent from our field observations immediately upstream of the lake or from satellite imagery, but riparian tree cover obscured views of most of the channel in the imagery. Earlier comparisons of WEPP and field data show that although generally performing acceptably, the model tended to underestimate erosion in severely burned areas (Fernández & Vega, 2018; Kampf et al., 2020; Larsen & MacDonald, 2007; Moffet et al., 2007; Robichaud et al., 2016; Spigel & Robichaud, 2007). Some of those underestimations (mostly in study sites <1 km^2) were attributed to post-fire debris flows, which export sediment by processes not represented in WEPP. Applying WEPP to a larger central California watershed (116 km^2) without anthropogenic land use, East et al. (2024) found that WEPP performed well, predicting 81%–106% of the measured sediment yield from a watershed burned at moderate to low soil burn severity, with the range being a function of density assumptions in the field results. Comparing WEPP output to field measurements in three burned watersheds around Whiskeytown Lake, northern California (13–29 km^2; East et al., 2021), Dow et al. (2024) determined that the ratios of modeled to measured sediment yield were 0.5, 1.5, and 3.7 for the three watersheds, respectively; thus, overestimation in two of three

23335084, 2025, 1, Downloaded from https://agupubs.onlinelibrary.wiley.com/doi/10.1029/2024EA003939, Wiley Online Library on [23/01/2025]. See the Terms and Conditions (https://onlinelibrary.wiley.com/terms-and-conditions) on Wiley Online Library for rules of use; OA articles are governed by the applicable Creative Commons License

23335084, 2025, 1, Downloaded from https://agupubs.onlinelibrary.wiley.com/doi/10.1029/2024EA003939, Wiley Online Library on [23/01/2025]. See the Terms and Conditions (https://onlinelibrary.wiley.com/terms-and-conditions) on Wiley Online Library for rules of use; OA articles are governed by the applicable Creative Commons License

basins but well within an order of magnitude and consistent with our findings from the second year of this study (overprediction by a factor of 1.9). Interestingly, when Miller et al. (2011) used WEPP to generate spatially explicit annualized post-fire erosion predictions across the western U.S., their estimates for the western Sierra Nevada were also an overprediction compared to our field results, ranging from 5,000 to 10,000 t/km^2 throughout our study region.

In addition to the possibility that hillslopes produced sediment that had not yet moved downstream to the reservoir (i.e., sediment represented in model results but not in our surveys), the model overpredicting sediment yield also may have been a function of where the snow line falls during winter storms. At an elevation of 1,050–1,790 m, the study area is in the part of the western Sierra Nevada where winter storms may bring rain, snow, or both, and in satellite imagery we observed many instances of the snow line being within this watershed or just above or below it (Figure 8). Being near the snow line could also explain the greater rain totals at Sly Park Dam than higher in the watershed (Figure 3). The gage at the dam measures rain-snow equivalent, whereas the gage on the higher-elevation ridge does not sense snowfall; during winter 2023 the gage on the ridge measured 75% of the total precipitation measured at the dam, with snow likely explaining the difference. The 4-km-scale gridded climatology used as input to WEPPcloud does include snowfall but may not be sensitive enough to represent daily snow versus rain accurately in this topographic transition zone; we ran the model using default parameters for snow elevation and snow density, not having sufficient information to support different selections. This may also explain the overpredictions for two of three Whiskeytown Lake watersheds (Dow et al., 2024; East et al., 2021) as those two included higher elevations than the third (up to 1,890 m).

It is not surprising that WEPP, or any model, would have difficulty predicting post-fire erosion accurately in a setting with heavily managed, rapidly changing forest cover and an elevation near the winter-storm snow line. However, for practical purposes, resource managers in the western U.S. often do apply WEPP (or ERMiT, which uses the WEPP processor; Robichaud et al., 2011) as part of post-fire hazard assessments; no currently existing model accounts for geomorphic disturbances of salvage logging. With that in mind, knowing how WEPP performed under these circumstances—predicting approximately double the measured sediment yield from a severely burned, salvage-logged 25-km^2 watershed in a wet year—will have management as well as scientific value in Sierra Nevada watersheds.

6. Conclusions

Research into wildfire and post-fire landscape change is growing rapidly as fire regimes intensify. There is still much to learn about how erosional responses develop as a function of landscape variables (steepness, soil type, lithology), precipitation, fire and soil burn severity, fuel conditions before the fire, and various post-fire management actions, some of which, including salvage logging, profoundly increase the geomorphic disturbance associated with a fire. We intend for this study and the others in this series—using reservoir sedimentation to evaluate post-fire sediment export at 10^1- to 10^2-km^2 watershed scale—to inform scientific investigations and resource management as California's landscapes and water infrastructure face a warming climate.

In the moderately to severely burned 25.4-km^2 forested Sly Park Creek watershed in the western Sierra Nevada, we detected lower sediment yield than the long-term average in the first year after the Caldor Fire (conservatively estimated at 21.8–28.0 t/km^2). First-year sediment export was low enough to be difficult to measure with our topographic and bathymetric survey methods, which are most effective where the ratio of the sedimentary signal to the noise (uncertainty) is large. In the second year post-fire the sediment delivery was much greater (1,560–2,010 t/km^2, an order of magnitude above long-term values indicated by bedrock denudation rates), attributed to a combination of greater precipitation and intensive salvage logging. No debris flows occurred in the study area. Simulations using the WEPP model overestimated the measured sediment yield in both years, although in the second year by a factor (1.9) that aligned with previously determined model performance in northern California. We encourage additional field data collection, and validation of erosion models where feasible, to further expand the range of conditions informing post-fire hazard assessments and management decisions.

Data Availability Statement

All data discussed in this paper are publicly available. Bathymetric survey data from Jenkinson Lake can be downloaded from Dartnell et al. (2024). Orthomosaic imagery and digital surface models from UAS surveys of

23335084, 2025, 1, Downloaded from https://agupubs.onlinelibrary.wiley.com/doi/10.1029/2024EA003939, Wiley Online Library on [23/01/2025]. See the Terms and Conditions (https://onlinelibrary.wiley.com/terms-and-conditions) on Wiley Online Library for rules of use; OA articles are governed by the applicable Creative Commons License

subaerially exposed parts of the lake can be downloaded from Logan and East (2024). The WEPPcloud graphical user interface (GUI) version of the WEPP model is available from https://wepp.cloud/weppcloud/ (open source). The Caldor Fire perimeter and soil burn severity maps used as input parameters to the model are available from the Monitoring Trends in Burn Severity (2024) website, https://mtbs.gov. Sentinel-2 satellite images in Figure 8 can be accessed from the European Space Agency at https://browser.dataspace.copernicus.eu/. The rainfall data from the gage at Sly Park Dam are available from the California Department of Water Resources (2023), and rainfall data from the gage in the upper Sly Park Creek watershed are available from Lindsay (2024).

Acknowledgments

This study was funded by supplemental appropriations from the U.S. Government to support post-disaster emergency assistance (Public Law 117-43, enacted in 2022), with oversight from the U.S. Geological Survey's Landslide Hazards Program. The authors are grateful for productive collaboration with Jason Kean and Matthew Thomas (U.S. Geological Survey) on post-fire research, and with Roger Lew and Mariana Dobre (University of Idaho) on the use of the WEPP model. Jordan Baxter, El Dorado Irrigation District hydrologist, provided helpful information on effects of the Caldor Fire on water-supply infrastructure in and around Jenkinson Lake. The manuscript was improved by constructive review comments from Jason W. Kean, Charles Shobe, and one anonymous reviewer. We thank Editor Graziella Caprarelli for handling the manuscript. Any use of trade, firm, or product names is for descriptive purposes only and does not imply endorsement by the U.S. government.

References

Abatzoglou, J. T. (2013). Development of gridded surface meteorological data for ecological applications and modelling. *International Journal of Climatology*, *33*(1), 121–131. https://doi.org/10.1002/joc.3413

Abatzoglou, J. T., & Williams, A. P. (2016). Impact of anthropogenic climate change on wildfire across western US forests. *Proceedings of the National Academy of Sciences of the United States of America*, *113*(42), 11770–11775. https://doi.org/10.1073/pnas.1607171113

Abatzoglou, J. T., Williams, A. P., & Barbero, R. (2019). Global emergence of anthropogenic climate change in fire weather indices. *Geophysical Research Letters*, *46*(1), 326–336. https://doi.org/10.1029/2018GL080959

Allan, R. P., & Soden, B. J. (2008). Atmospheric warming and the amplification of precipitation extremes. *Science*, *321*(5895), 1481–1484. https://doi.org/10.1126/science.1160787

Anderson, S. W. (2019). Uncertainty in quantitative analyses of topographic change: Error propagation and the role of thresholding. *Earth Surface Processes and Landforms*, *44*(5), 1015–1033. https://doi.org/10.1002/esp.4551

Asner, G. P., Brodrick, P. G., Anderson, C. B., Vaughn, N., Knapp, D. E., & Martin, R. E. (2015). Progressive forest canopy water loss during the 2012–2015 California drought. *Proceedings of the National Academy of Sciences of the United States of America*, E249–E255. https://doi.org/10.1073/pnas.1523397113

Basso, M., Mateus, M., Ramos, T. B., & Vieira, D. C. S. (2021). Potential post-fire impacts on a water supply reservoir: An integrated watershed-reservoir approach. *Frontiers in Environmental Science*, *9*, 684703. https://doi.org/10.3389/fenvs.2021.684703

Beck, H. E., McVicar, T. R., Vergopolan, N., Berg, A., Lutsko, N., Dufour, A., et al. (2023). High-resolution (1 km) Köppen-Geiger maps for 1901–2099 based on constrained CMIP6 projections. *Scientific Data*, *10*(1), 724. https://doi.org/10.1038/s41597-023-02549-6

Belongia, M. F., Wagner, C. H., Seipp, K. Q., & Ajami, N. K. (2023). Building water resilience in the face of cascading wildfire risks. *Science Advances*, *9*(37), eadf9534. https://doi.org/10.1126/sciadv.adf9534

Boer, M. M., Resco de Dios, V., & Bradstock, R. A. (2020). Unprecedented burn area of Australian mega forest fires. *Nature Climate Change*, *10*(3), 170–172. https://doi.org/10.1038/s41558-020-0716-1

Bureau of Reclamation. (2024). Sly Park Dam. Retrieved from https://www.usbr.gov/projects/index.php?id=246

California Board of Forestry and Fire Protection. (2024). California forest practice rules. Retrieved from https://bof.fire.ca.gov/regulations/bills-statutes-rules-and-annual-california-forest-practice-rules/

California Department of Forestry and Fire Protection (CalFire). (2023). Caldor Fire. Retrieved from https://www.fire.ca.gov/incidents/2021/8/14/caldor-fire

California Department of Water Resources. (2023). Rainfall data downloaded from the California data exchange center. Retrieved from http://cdec.water.ca.gov

California Office of Emergency Services. (2024). Fire integrated real-time Intelligence system program (FIRIS). Retrieved from https://www.caloes.ca.gov/office-of-the-director/operations/response-operations/fire-rescue/firis/

Callahan, R. P., Ferrier, K. L., Dixon, J., Dosseto, A., Hahm, W. J., Jessup, B. S., et al. (2019). Arrested development: Erosional equilibrium in the southern Sierra Nevada, California, maintained by feedbacks between channel incision and hillslope sediment production. *Geological Society of America Bulletin*, *131*(7–8), 1179–1202. https://doi.org/10.1130/B35006.1

Cerdà, A., Imeson, A. C., & Calvo, A. (1995). Fire and aspect induced differences on the erodibility and hydrology of soils at La Costera, Valencia, southeast Spain. *Catena*, *24*(4), 289–304. https://doi.org/10.1016/0341-8162(95)00031-2

Cerdà, A., & Lasanta, T. (2005). Long-term erosional responses after fire in the Central Spanish Pyrenees: 1. Water and sediment yield. *Catena*, *60*(1), 59–80. https://doi.org/10.1016/j.catena.2004.09.006

Chin, A., Burton, J. W., Humphreys, K. M., Florsheim, J. L., Kinoshita, A. M., Andreano, E. C., & Eckermann, T. K. (2024). Vegetation and channel recovery ten years following the Waldo Canyon Fire of Colorado. In J. L. Florsheim, A. P. O'Dowd, & A. Chin (Eds.), *Biogeomorphic responses to wildfire in fluvial ecosystems. Geological Society of America Special Paper 562* (pp. 27–42). https://doi.org/10.1130/2024.2562(02)

Chin, A., Solverson, A. P., O'Down, A. P., Florsheim, J. L., Kinoshita, A. M., Nourbakhshbeidokhti, S., et al. (2019). Interacting geomorphic and ecological response of step-pool streams after wildfire. *Geological Society of America Bulletin*, *131*, 1480–1500. https://doi.org/10.1130/B35049.1

Cole, R. P., Bladon, K. D., Wagenbrenner, J. W., & Coe, D. B. R. (2021). Hillslope sediment production after wildfire and post-fire forest management in northern California. *Hydrological Processes*, *34*(26), 5242–5259. https://doi.org/10.1002/hyp.13932

Conroy, J. L., Overpeck, J. T., Cole, J. E., Shanahan, T. M., & Steinitz-Kannan, M. (2008). Holocene changes in eastern tropical Pacific climate inferred from a Galápagos lake sediment record. *Quaternary Science Reviews*, *27*(11–12), 1133–1180. https://doi.org/10.1016/j.quascirev.2008.02.015

Cunningham, C. X., Williamson, G. J., & Bowman, D. M. J. S. (2024). Increasing frequency and intensity of the most extreme wildfires on Earth. *Nature Ecology & Evolution*, *8*(8), 1420–1425. https://doi.org/10.1038/s41559-024-02452-2

Dartnell, P., East, A. E., Logan, J., Hatcher, G. A., Currie, J. E., Marcuson, R. K., et al. (2024). Bathymetry and acoustic backscatter data for Jenkinson Lake, California collected during three USGS field activities, 2022-604-FA, 2022-649-FA, and 2023-634-FA [Dataset]. *U.S. Geological Survey data release*. https://doi.org/10.5066/P13BSSDY

DeBano, L. F. (2000). The role of fire and soil heating on water repellency in wildland environments: A review. *Journal of Hydrology*, *231–232*, 195–206. https://doi.org/10.1016/s0022-1694(00)00194-3

DeLong, S. B., Youberg, A. M., DeLong, W. M., & Murphy, B. P. (2018). Post-wildfire landscape change and erosional processes from repeat terrestrial lidar in a steep headwater catchment, Chiricahua Mountains, Arizona, USA. *Geomorphology*, *300*, 13–30. https://doi.org/10.1016/j.geomorph.2017.09.028

Dobre, M., Srivastava, A., Lew, R., Deval, C., Brooks, E. S., Elliot, W. J., & Robichaud, P. R. (2022). WEPPcloud: An online watershed-scale hydrologic modeling tool. Part II. Model performance assessment and applications to forest management and wildfires. *Journal of Hydrology*, 127776. https://doi.org/10.1016/j.jhydrol.2022.127776

Dow, H. W., East, A. E., Sankey, J. B., Warrick, J. A., Kostelnik, J., Lindsay, D., & Kean, J. (2024). Postfire sediment mobilization and its downstream implications across California, 1984–2021. *Journal of Geophysical Research: Earth Surface*, *129*(8). https://doi.org/10.1029/2024JF007725

East, A. E., Logan, J. B., Dartnell, P., Lieber-Kotz, O., Cavagnaro, D. B., McCoy, S. W., & Lindsay, D. N. (2021). Watershed sediment yield following the 2018 Carr Fire, Whiskeytown National Recreation Area, northern California. *Earth and Space Science*, *8*(9), e2021EA001828. https://doi.org/10.1029/2021EA001828

East, A. E., Logan, J. B., Dow, H. W., Smith, D. P., Iampietro, P., Warrick, J. A., et al. (2024). Post-fire sediment yield from a central California watershed: Field measurements and validation of the WEPP model. *Earth and Space Science*, *11*(7). https://doi.org/10.1029/2024EA003575

East, A. E., & Sankey, J. B. (2020). Geomorphic and sedimentary effects of modern climate change: Current and anticipated future conditions in the western United States. *Reviews of Geophysics*, *58*(4), e2019RG000692. https://doi.org/10.1029/2019RG000692

Ebel, B. A., & Moody, J. A. (2017). Synthesis of soil-hydraulic properties and infiltration timescales in wildfire-affected soils. *Hydrological Processes*, *31*(2), 324–340. https://doi.org/10.1002/hyp.10998

Ebel, B. A., Shephard, Z. M., Walvoord, M. A., Murphy, S. F., Partridge, T. F., & Perkins, K. S. (2023). Modeling post-wildfire hydrologic response: Review and future directions for applications of physically based distributed simulation. *Earth's Future*, *11*(2), e2022EF003038. https://doi.org/10.1029/2022EF003038

Ebel, B. A., Wagenbrenner, J. W., Kinoshita, A. M., & Bladon, K. D. (2022). Hydrologic recovery after wildfire: A framework of approaches, metrics, criteria, trajectories, and timescales. *Journal of Hydrology and Hydromechanics*, *70*(4), 388–400. https://doi.org/10.2478/johh-2022-0033

Ellett, N. G., Pierce, J. L., & Glenn, N. F. (2019). Partitioned by process: Measuring post-fire debris-flow and rill erosion with structure from motion photogrammetry. *Earth Surface Processes and Landforms*, *44*(15), 3128–3146. https://doi.org/10.1002/esp.4728

Elliott, S. M., Hornberger, M. I., Rosenberry, D. O., Frus, R. J., & Webb, R. M. (2024). A conceptual framework to assess post-wildfire water quality: State of the science and knowledge gaps. *Water Resources Research*, *60*(7), e2023WR036260. https://doi.org/10.1029/2023WR036260

Fernández, C., & Vega, J. A. (2018). Evaluation of the RUSLE and disturbed WEPP erosion models for predicting soil loss in the first year after wildfire in NW Spain. *Environmental Research*, *165*, 279–285. https://doi.org/10.1016/j.envres.2018.04.008

Feurdean, A., Florescu, G., Tantau, I., Vanniere, B., Diaconu, A.-C., Pfeiffer, M., et al. (2020). Recent fire regime in the southern boreal forests of western Siberia is unprecedented in the last five millennia. *Quaternary Science Reviews*, *244*, 106495. https://doi.org/10.1016/j.quascirev.2020.106495

Fish, M. A., Wilson, A. M., & Ralph, F. M. (2019). Atmospheric river families: Definition and associated synoptic conditions. *Journal of Hydrometeorology*, *20*(10), 2091–2107. https://doi.org/10.1175/JHM-D-18-0217.1

Flanagan, D. C., Gilley, J. E., & Franti, T. G. (2007). Water erosion prediction project (WEPP): Development history, model capabilities, and future enhancements. *Transactions of the American Society of Agricultural and Biological Engineers*, *50*, 1603–1612.

Flanagan, D. C., & Nearing, M. A. (1995). *USDA—Water erosion prediction project hillslope profile and watershed model documentation 1*. U.S. Department of Agriculture, Agricultural Research Service, National Soil Erosion Research Laboratory Report No. 10.

Florsheim, J. L., & Chin, A. (2023). Disturbance and recovery of physical elements of habitat in relation to post-wildfire channel sedimentation, southern California Transverse Ranges. In J. L. Florsheim, A. P. O'Dowd, & A. Chin (Eds.), *Biogeomorphic Responses to Wildfire in Fluvial Ecosystems: Geological Society of America Special Paper 562* (pp. 57–77). https://doi.org/10.1130/2024.2562(04)

Florsheim, J. L., Chin, A., Kinoshita, A. M., & Nourbakhshbeidokhti, S. (2017). Effect of storms during drought on post-wildfire recovery of channel sediment dynamics and habitat in the southern California chaparral, USA. *Earth Surface Processes and Landforms*, *42*(10), 1482–1492. https://doi.org/10.1002/esp.4117

Florsheim, J. L., Keller, E. A., & Best, D. W. (1991). Fluvial sediment transport in response to moderate storm flows following chaparral wildfire, Ventura County, southern California. *Geological Society of America Bulletin*, *103*(4), 504–511. https://doi.org/10.1130/0016-7606(1991)103<0504:fstirt>2.3.co;2

Goode, J. R., Luce, C. H., & Buffington, J. M. (2012). Enhanced sediment delivery in a changing climate in semi-arid mountain basins: Implications for water resource management and aquatic habitat in the northern Rocky Mountains. *Geomorphology*, *139–140*, 1–15. https://doi.org/10.1016/j.geomorph.2011.06.021

Goss, M., Swain, D. L., Abatzoglou, J. T., Sarhadi, A., Kolden, C. A., Williams, A. P., & Diffenbaugh, N. S. (2020). Climate change is increasing the likelihood of extreme autumn wildfire conditions across California. *Environmental Research Letters*, *15*(9), 094016. https://doi.org/10.1088/1748-9326/ab83a7

Guilinger, J. J., Foufoula-Georgiou, E., Gray, A. B., Randerson, J. T., Smyth, P., Barth, N. C., & Goulden, M. L. (2023). Predicting postfire sediment yields of small steep catchments using airborne lidar differencing. *Geophysical Research Letters*, *50*(16), e2023GL104626. https://doi.org/10.1029/2023GL104626

Guilinger, J. J., Gray, A. B., Barth, N. C., & Fong, B. T. (2020). The evolution of sediment sources over a sequence of postfire sediment-laden flows revealed through repeat high-resolution change detection. *Journal of Geophysical Research: Earth Surface*, *125*(10), e2020JF005527. https://doi.org/10.1029/2020JF005527

Gutierrez, A. A., Hantson, S., Langenbrunner, B., Chen, B., Jin, Y., Goulden, M. L., & Randerson, J. T. (2021). Wildfire response to changing daily temperature extremes in California's Sierra Nevada. *Science Advances*, *7*(47), eabe6417. https://doi.org/10.1126/sciadv.abe6417

Hallema, D. W., Robinne, F.-N., & Bladon, K. D. (2018). Reframing the challenge of global wildfire threats to water supplies. *Earth's Future*, *6*, 772–776. https://doi.org/10.1029/2018EF000867

Huang, X., Swain, D. L., & Hall, A. D. (2020). Future precipitation increase from very high resolution ensemble downscaling of extreme atmospheric river storms in California. *Science Advances*, *6*(29), eaba1323. https://doi.org/10.1126/sciadv.aba1323

Intergovernmental Panel on Climate Change (IPCC). (2014). Climate change 2014: Synthesis report. In Core Writing Team, R. K. Pachauri, & L. A. Meyer (Eds.), *Contribution of working groups I, II and III to the Fifth Assessment Report of the Intergovernmental Panel on Climate Change* (p. 151). IPCC. Retrieved from https://www.ipcc.ch/report/ar5/syr/

Jain, P., Sharma, A. R., Acuna, D. C., Abatzoglou, J. T., & Flannigan, M. (2024). Record-breaking fire weather in North America in 2021 was initiated by the Pacific northwest heat dome. *Nature Communications Earth & Environment*, *5*(1), 202. https://doi.org/10.1038/s43247-024-01346-2

Jennings, C. W., Gutierrez, C., Bryant, W., Saucedo, G., & Wills, C. (2010). *Geologic map of Cailfornia*. California Geological Survey. Geologic Data Map GDM-2.2010, scale 1:750,000. Retrieved from https://ngmdb.usgs.gov/Prodesc/proddesc_96750.htm

23335084, 2025, 1, Downloaded from https://agupubs.onlinelibrary.wiley.com/doi/10.1029/2024EA003939, Wiley Online Library on [23/01/2025]. See the Terms and Conditions (https://onlinelibrary.wiley.com/terms-and-conditions) on Wiley Online Library for rules of use; OA articles are governed by the applicable Creative Commons License

Jin, S., Homer, C., Yang, L., Danielson, P., Dewitz, J., Li, C., et al. (2019). Overall methodology design for the United States National land cover database 2016 products. *Remote Sensing*, *11*(24), 2971. https://doi.org/10.3390/rs11242971

Jonas, J. L., Berryman, E., Wolk, B., Morgan, P., & Robichaud, P. R. (2019). Post-fire wood mulch for reducing erosion potential increases tree seedlings with few impacts on understory plants and soil nitrogen. *Forest Ecology and Management*, *453*, 117567. https://doi.org/10.1016/j.foreco.2019.117567

Jones, M. W., Abatzoglou, J. T., Veraverbeke, S., Andela, N., Lasslop, G., Forkel, M., et al. (2022). Global and regional trends and drivers of fire under climate change. *Reviews of Geophysics*, *60*(3), e2020RG000726. https://doi.org/10.1029/2020RG000726

Jong-Levinger, A., Banerjee, T., Houston, D., & Sanders, B. F. (2022). Compound post-fire flood hazards considering infrastructure sedimentation. *Earth's Future*, *10*(8), e2022EF002670. https://doi.org/10.1029/2022EF002670

Jong-Levinger, A., Houston, D., & Sanders, B. F. (2024). Estimating post-fire flood infrastructure clogging and overtopping hazards. *Water Resources Research*, *60*(8), e2023WR036522. https://doi.org/10.1029/2023WR036522

Juang, C. S., Williams, A. P., Abatzoglou, J. T., Balch, J. K., Hurteau, M. D., & Moritz, M. A. (2022). Rapid growth of large forest fires drives the exponential response of annual forest-fire area to aridity in the western United States. *Geophysical Research Letters*, *49*(5), e2021GL097131. https://doi.org/10.1029/2021GL097131

Jumps, N., Gray, A. B., Guilinger, J. J., & Cowger, W. C. (2022). Wildfire impacts on the persistent suspended sediment dynamics of the Ventura River, California. *Journal of Hydrology: Regional Studies*, *41*, 101096. https://doi.org/10.1016/j.ejrh.2022.101096

Kampf, S. K., Gannon, B. M., Wilson, C., Saavedra, F., Miller, M. E., Heldmyer, A., et al. (2020). PEMIP: Post-fire erosion model intercomparison project. *Journal of Environmental Management*, *268*, 110704. https://doi.org/10.1016/j.jenvman.2020.110704

KCRA News. (2022). "Stark reminder of what can happen to your watershed": How high-intensity wildfires impact water quality years after the smoke clear. Article published 17 June 2022 Retrieved from https://www.kcra.com/article/how-high-intensity-wildfires-impact-water-quality-years-after-smoke-clears/40315113

Kean, J. W., & Staley, D. M. (2021). Forecasting the frequency and magnitude of postfire debris flows across southern California. *Earth's Future*, *9*(3), e2020EF001735. https://doi.org/10.1029/2020EF001735

Kean, J. W., Staley, D. M., & Cannon, S. H. (2011). In situ measurements of post-fire debris flows in southern California: Comparisons of the timing and magnitude of 24 debris-flow events with rainfall and soil moisture conditions. *Journal of Geophysical Research*, *116*(F4), F04019. https://doi.org/10.1029/2011JF002005

Kean, J. W., Staley, D. M., Lancaster, J. T., Rengers, F. K., Swanson, B. J., Coe, J. A., et al. (2019). Inundation, flow dynamics, and damage in the 9 January 2018 Montecito debris-flow event, California, USA: Opportunities and challenges for post-wildfire risk assessment. *Geosphere*, *15*(4), 1140–1163. https://doi.org/10.1130/ges02048.1

Keeley, J. E., & Syphard, A. D. (2016). Climate change and future fire regimes: Examples from California. *Geosciences*, *6*(3), 37. https://doi.org/10.3390/geosciences6030037

Keizer, J. J., Silva, F. C., Vieira, D. C. S., González-Pelayo, O., Campos, I., Vieira, A. M. D., et al. (2018). The effectiveness of two contrasting mulch application rates to reduce post-fire erosion in a Portuguese eucalypt plantation. *Catena*, *169*, 21–30. https://doi.org/10.1016/j.catena.2018.05.029

Keller, E. A., Valentine, D. W., & Gibbs, D. R. (1997). Hydrological response of small watersheds following the Southern California Painted Cave Fire of June 1990. *Hydrological Processes*, *11*(4), 401–414. https://doi.org/10.1002/(sici)1099-1085(19970330)11:4<401::aid-hyp447>3.3.co;2-g

Kemter, M., Fischer, M., Luna, L. V., Schönfeldt, E., Vogel, J., Banerjee, A., et al. (2021). Cascading hazards in the aftermath of Australia's 2019/2020 Black Summer wildfires. *Earth's Future*, *9*(3), e2020EF001884. https://doi.org/10.1029/2020EF001884

Kinoshita, A. M., & Hogue, T. S. (2011). Spatial and temporal controls on post-fire hydrologic recovery in Southern California watersheds. *Catena*, *87*(2), 240–252. https://doi.org/10.1016/j.catena.2011.06.005

Kolden, C. A., Abatzoglou, J. T., Jones, M. W., & Jain, P. (2024). Wildfires in 2023. *Nature Reviews Earth & Environment*, *5*(4), 238–240. https://doi.org/10.1038/s43017-024-00544-y

Laflen, J. M., Elliot, W. J., Flanagan, D. C., Meyer, C. R., & Nearing, M. A. (1997). WEPP-Predicting water erosion using a process-based model. *Journal of Soil and Water Conservation*, *52*, 96–102.

Laflen, J. M., Lane, L. J., & Foster, G. R. (1991). WEPP: A new generation of erosion prediction technology. *Journal of Soil and Water Conservation*, *46*, 34–38.

Lancaster, J. T., Swanson, B. J., Lukashov, S. G., Oakley, N. S., Lee, J. B., Spangler, E. R., et al. (2021). Observations and analyses of the 9 January 2018 debris-flow disaster, Santa Barbara County, California. *Environmental and Engineering Geoscience*, *27*(1), 3–27. https://doi.org/10.2113/eeg-d-20-00015

Lane, P. N. J., Sheridan, G. J., & Noske, P. J. (2006). Changes in sediment loads and discharge from small mountain catchments following wildfire in south eastern Australia. *Journal of Hydrology*, *331*(3–4), 495–510. https://doi.org/10.1016/j.jhydrol.2006.05.035

Larsen, I. J., & MacDonald, L. H. (2007). Predicting postfire sediment yields at the hillslope scale: Testing RUSLE and Disturbed WEPP. *Water Resources Research*, *43*(11). https://doi.org/10.1029/2006WR005560

Lew, R., Dobre, M., Srivastava, A., Brooks, E. S., Elliot, W. J., Robichaud, P. R., & Flanagan, D. C. (2022). WEPPcloud: An online watershed-scale hydrologic modeling tool. Part I. Model description. *Journal of Hydrology*, *608*, 127603. https://doi.org/10.1016/j.jhydrol.2022.127603

Lindsay, D. N. (2024). Daily rainfall totals (mm) Sly Park Creek—Caldor Fire [Dataset]. https://doi.org/10.5281/zenodo.13272989

Littell, J. S., McKenzie, D., Wan, H. Y., & Cushman, S. A. (2018). Climate change and future wildfire in the western United States: An ecological approach to nonstationarity. *Earth's Future*, *6*(8), 1097–1111. https://doi.org/10.1029/2018EF000878

Logan, J. B., & East, A. E. (2024). Digital surface models and orthomosaic images from UAS surveys of Jenkinson Lake, El Dorado County [Dataset]. *CA: U.S. Geological Survey data release*. https://doi.org/10.5066/P14QWDYN

Lopes, A. R., Girona-García, A., Corticeiro, S., Martins, R., Keizer, J. J., & Vieira, D. C. S. (2021). What is wrong with post-fire soil erosion modelling? A meta-analysis on current approaches, research gaps, and future directions. *Earth Surface Processes and Landforms*, *46*(1), 205–219. https://doi.org/10.1002/esp.5020

Los Angeles County. (2021). *Devil's gate reservoir restoration project*. Los Angeles County Public Works Department. Retrieved from https://pw.lacounty.gov/swe/DevilsGate/

Los Angeles County. (2023). *Santa Anita Reservoir post-fire emergency restoration project*. Los Angeles County Public Works Department. Retrieved from https://pw.lacounty.gov/wrd/Projects/Bobcatfire/santaanita.shtml

Luković, J., Chiang, J. C. H., Blagojević, D., & Sekulić, A. (2021). A later onset of the rainy season in California. *Geophysical Research Letters*, *48*(4), e2020GL090350. https://doi.org/10.1029/2020GL090350

MacDonald, G., Wall, T., Enquist, C. A. F., LeRoy, S. R., Bradford, J. B., Breshears, D. D., et al. (2023). Drivers of California's changing wildfires: A state-of-the-knowledge synthesis. *International Journal of Wildland Fire*, *32*(7), 1039–1058. https://doi.org/10.1071/WF22155

23335084, 2025, 1, Downloaded from https://agupubs.onlinelibrary.wiley.com/doi/10.1029/2024EA003939, Wiley Online Library on [23/01/2025]. See the Terms and Conditions (https://onlinelibrary.wiley.com/terms-and-conditions) on Wiley Online Library for rules of use; OA articles are governed by the applicable Creative Commons License

McGuire, L. A., Ebel, B. A., Rengers, F. K., Vieira, D. C. S., & Nyman, P. (2024). Fire effects on geomorphic processes. *Nature Reviews Earth & Environment*, *5*(7), 486–503. https://doi.org/10.1038/s43017-024-00557-7

McGuire, L. A., & Youberg, A. M. (2020). What drives spatial variability in rainfall intensity-duration thresholds for post-wildfire debris flows? Insights from the 2018 Buzzard Fire, NM, USA. *Landslides*, *17*(10), 2385–2399. https://doi.org/10.1007/s10346-020-01470-y

Melia, N., Dean, S., Pearce, H. G., Harrington, L., Frame, D. J., & Strand, T. (2022). Aotearoa New Zealand's 21st-century wildfire climate. *Earth's Future*, *10*(6), e2022EF002853. https://doi.org/10.1029/2022EF002853

Menounos, B., & Clague, J. J. (2008). Reconstructing hydro-climatic events and glacier fluctuations over the past millennium from annually laminated sediments of Cheakamus Lake, southern Coast Mountains, British Columbia, Canada. *Quaternary Science Reviews*, *27*(7–8), 701–713. https://doi.org/10.1016/j.quascirev.2008.01.007

Miller, M. E., MacDonald, L. H., Robichaud, P. R., & Elliot, W. J. (2011). Predicting post-fire hill slope erosion in forest lands of the western United States. *International Journal of Wildland Fire*, *20*(8), 982–999. https://doi.org/10.1071/WF09142

Miner, K. R., Turetsky, M. R., Malina, E., Bartsch, A., Tamminen, J., McGuire, A. D., et al. (2022). Permafrost carbon emissions in a changing Arctic. *Nature Reviews Earth & Environment*, *3*(1), 55–67. https://doi.org/10.1038/s43017-021-00230-3

Moffet, C. A., Pierson, F. B., Robichaud, P. R., Spaeth, K. E., & Hardegree, S. P. (2007). Modeling soil erosion on steep sagebrush rangeland before and after prescribed fire. *Catena*, *71*(2), 218–228. https://doi.org/10.1016/j.catena.2007.03.008

Monitoring Trends in Burn Severity (MTBS). (2024). *Monitoring trends in burn severity, interagency website maintained by U.S. Department of Agriculture*. U.S. Forest Service, U.S. Department of Interior, and U.S. Geological Survey.

Moody, J. A., & Martin, D. A. (2009). Synthesis of sediment yields after wildland fire in different rainfall regimes in the western United States. *International Journal of Wildland Fire*, *18*(1), 96–115. https://doi.org/10.1071/WF07162

Moody, J. A., Shakesby, R. A., Robichaud, P. R., Cannon, S. H., & Martin, D. A. (2013). Current research issues related to post-wildfire runoff and erosion processes. *Earth-Science Reviews*, *122*, 10–37. https://doi.org/10.1016/j.earscirev.2013.03.004

Morán-Ordóñez, A., Duane, A., Gil-Tena, A., De Cáceres, M., Aquilué, N., Guerra, C. A., et al. (2020). Future impact of climate extremes in the Mediterranean: Soil erosion projections when fire and extreme rainfall meet. *Land Degradation & Development*, *31*(18), 3040–3054. https://doi.org/10.1002/ldr.3694

Murphy, B. P., Yocom, L. L., & Belmont, P. (2018). Beyond the 1984 perspective: Narrow focus on modern wildfire trends underestimates future risks to water security. *Earth's Future*, *6*(11), 1492–1497. https://doi.org/10.1029/2018EF001006

Murphy, S. F., Alpers, C. N., Anderson, C. W., Banta, J. R., Blake, J. M., Carpenter, K. D., et al. (2023). A call for strategic water-quality monitoring to advance assessment and prediction of wildfire impacts on water supplies. *Frontiers in Water*, *5*, 1144225. https://doi.org/10.3389/frwa.2023.1144225

National Oceanic and Atmospheric Administration. (2024). California Nevada River Forecast Center, Observed Precipitation Interactive Map Interface. Retrieved from https://www.cnrfc.noaa.gov/ol.php?type=precip

Nitzsche, N., Nunes, J. P., & Parente, J. (2024). Assessing post-fire water quality changes in reservoirs: Insights from a large dataset in Portugal. *Science of the Total Environment*, *912*, 169463. https://doi.org/10.1016/j.scitotenv.2023.169463

Noske, P. J., Nyman, P., Lane, P. N. J., Rengers, F. K., & Sheridan, G. J. (2024). Changes in soil erosion caused by wildfire: A conceptual biogeographic model. *Geomorphology*, *459*, 109272. https://doi.org/10.1016/j.geomorph.2024.109272

Oakley, N. S. (2021). A warming climate adds complexity to post-fire hydrologic hazard planning. *Earth's Future*, *9*(7), e2021EF002149. https://doi.org/10.1029/2021EF002149

Olsen, W. H., Wagenbrenner, J. W., & Robichaud, P. R. (2021). Factors affecting connectivity and sediment yields following wildfire and post-fire salvage logging in California's Sierra Nevada. *Hydrological Processes*, *35*(1). https://doi.org/10.1002/hyp.13984

Ouyang, C., Xiang, W., An, H., Wang, F., Yang, W., & Fan, J. (2023). Mechanistic analysis and numerical simulation of the 2021 post-fire debris flow in Xiangjiao catchment, China. *Journal of Geophysical Research: Earth Surface*, *128*(1), e2022JF006846. https://doi.org/10.1029/2022JF006846

Parks, S. A., & Abatzoglou, J. T. (2020). Warmer and drier fire seasons contribute to increases in area burned at high severity in western US forests from 1985 to 2017. *Geophysical Research Letters*, *47*(22), e2020GL089858. https://doi.org/10.1029/2020GL089858

Paul, M. J., LeDuc, S. D., Lassiter, M. G., Moorhead, L. C., Noyes, P. D., & Leibowitz, S. G. (2022). Wildfire induces changes in receiving waters: A review with considerations for water quality management. *Water Resources Research*, *58*(9), e2021WR030699. https://doi.org/10.1029/2021WR030699

Pelletier, J. D., & Orem, C. A. (2014). How do sediment yields from post-wildfire debris-laden flows depend on terrain slope, burn severity class, and drainage basin area? Insights from airborne-LiDAR change detection. *Earth Surface Processes and Landforms*, *39*(13), 1822–1832. https://doi.org/10.1002/esp.3570

Prats, S. A., Malvar, M. C., & Wagenbrenner, J. W. (2021). Compaction and cover effects of runoff and erosion in post-fire salvage logged areas in the Valley Fire, California. *Hydrological Processes*, *35*(1). https://doi.org/10.1002/hyp.13997

Prein, A. F., Coen, J., & Jaye, A. (2022). The character and changing frequency of extreme California fire weather. *Journal of Geophysical Research: Atmospheres*, *127*(9), e2021JD035350. https://doi.org/10.1029/2021JD035350

Ramos-Scharrón, C. E., & LaFevor, M. C. (2018). Effects of forest roads on runoff initiation in low-order ephemeral streams. *Water Resources Research*, *54*(11), 8613–8631. https://doi.org/10.1029/2018WR023442

Randle, T. J., Morris, G. L., Tullos, D. D., Weirich, F. H., Kondolf, G. M., Moriasi, D. N., et al. (2021). Sustaining United States reservoir storage capacity: Need for a new paradigm. *Journal of Hydrology*, *602*, 126686. https://doi.org/10.1016/j.jhydrol.2021.126686

Rengers, F. K., McGuire, L. A., Kean, J. W., Staley, D. M., Dobre, M., Robichaud, P. R., & Swetnam, T. (2021). Movement of sediment through a burned landscape: Sediment volume observations and model comparisons in the San Gabriel Mountains, California, USA. *Journal of Geophysical Research: Earth Surface*, *126*(7), e2020JF006053. https://doi.org/10.1029/2020JF006053

Reybold, W. U., & TeSelle, G. W. (1989). Soil geographic data bases. *Journal of Soil and Water Conservation*, *44*, 28–29.

Robichaud, P. R., Elliot, W. J., Lewis, S. A., & Miller, M. E. (2016). Validation of a probabilistic post-fire erosion model. *International Journal of Wildland Fire*, *25*(3), 337–350. https://doi.org/10.1071/WF14171

Robichaud, P. R., Elliot, W. J., & Wagenbrenner, J. W. (2011). Probabilistic soil erosion modeling using the Erosion Risk Management Tool (ERMIT) after wildfires. In *ISELE Paper Number 11039. Paper Presented at the International Symposium on Erosion and Landscape Evolution; September 18–21, 2011; Anchorage, AK* (p. 8). ASABE Publication Number 711P0311cd Retrieved from https://www.fs.usda.gov/research/treesearch/41494

Robichaud, P. R., Storrar, K. A., & Wagenbrenner, J. W. (2019). Effectiveness of straw bale check dams at reducing post-fire sediment yield from steep ephemeral channels. *Science of the Total Environment*, *676*, 721–731. https://doi.org/10.1016/j.scitotenv.2019.04.246

Robichaud, P. R., Wagenbrenner, J. W., & Brown, R. E. (2010). Rill erosion in natural and disturbed forests: 1. Measurements. *Water Resources Research*, *46*(10), W10506. https://doi.org/10.1029/2009wr008314

23335084, 2025, 1, Downloaded from https://agupubs.onlinelibrary.wiley.com/doi/10.1029/2024EA003939, Wiley Online Library on [23/01/2025]. See the Terms and Conditions (https://onlinelibrary.wiley.com/terms-and-conditions) on Wiley Online Library for rules of use; OA articles are governed by the applicable Creative Commons License

Rogers, B. M., Balch, J. K., Goetz, S. J., Lehmann, C. E. R., & Turetsky, M. (2020). Focus on changing fire regimes: Interactions with climate, ecosystems, and society. *Environmental Research Letters*, *15*(3), 030201. https://doi.org/10.1088/1748-9326/ab6d3a

Ryan, S. E., Shobe, C. M., Rathburn, S. L., & Dixon, M. K. (2024). Suspended-sediment response to wildfire and a major post-fire flood on the Colorado Front Range. *River Research and Applications*, *40*(7), 1256–1272. https://doi.org/10.1002/rra.4286

Sankey, J. B., Kreitler, J., Hawbaker, T. J., McVay, J. L., Miller, M. E., Mueller, E. R., et al. (2017). Climate, wildfire, and erosion ensemble foretells more sediment in western USA watersheds. *Geophysical Research Letters*, *44*(17), 8884–8892. https://doi.org/10.1002/2017GL073979

Santi, P. M., & Rengers, F. K. (2020). Wildfire and landscape change. *Treatise on Geomorphology*, *13*, 262–287. https://doi.org/10.1016/B978-0-12-818234-5.00017-1

Shakesby, R. A., & Doerr, S. H. (2006). Wildfire as a hydrological and geomorphological agent. *Earth-Science Reviews*, *74*(3–4), 269–307. https://doi.org/10.1016/j.earscirev.2005.10.006

Sierra-Hernández, M. R., Beaudon, E., Porter, S. E., Mosley-Thompson, E., & Thompson, L. G. (2022). Increased fire activity in Alaska since the 1980s: Evidence from an ice core-derived black carbon record. *Journal of Geophysical Research: Atmospheres*, *127*(2), e2021JD035668. https://doi.org/10.1029/2021JD035668

Smith, S. G., Wegmann, K. W., Leithold, E. L., & Bohnenstiehl, D. R. (2019). A 4000-year record of hydrologic variability from the Olympic Mountains, Washington, USA. *The Holocene*, *29*(8), 1273–1291. https://doi.org/10.1177/0959683619846975

Snyder, N. P., Wright, S. A., Alpers, C. N., Flint, L. E., Holmes, C. W., & Rubin, D. M. (2006). Reconstructing depositional processes and history from reservoir stratigraphy: Englebright Lake, Yuba River, northern California. *Journal of Geophysical Research*, *111*(F4), F04003. https://doi.org/10.1029/2005JF000451

Spigel, K. M., & Robichaud, P. R. (2007). First-year post-fire erosion rates in Bitterroot National Forest, Montana. *Hydrological Processes*, *21*(8), 998–1005. https://doi.org/10.1002/hyp.6295

Staley, D. M., Kean, J. W., Cannon, S. H., Schmidt, K. M., & Laber, J. L. (2013). Objective definition of rainfall intensity-duration thresholds for the initiation of post-fire debris flows in Southern California. *Landslides*, *10*(5), 547–562. https://doi.org/10.1007/s10346-012-0341-9

Staley, D. M., Negri, J. A., Kean, J. W., Laber, J. L., Tillery, A. C., & Youberg, A. M. (2017). Prediction of spatially explicit rainfall intensity-duration thresholds for post-fire debris-flow generation in the western United States. *Geomorphology*, *278*, 149–162. https://doi.org/10.1016/j.geomorph.2016.10.019

Stock, G. M., Anderson, R. S., & Finkel, R. C. (2005). Rates of erosion and topographic evolution of the Sierra Nevada, California, inferred from cosmogenic ^{26}Al and ^{10}Be concentrations. *Earth Surface Processes and Landforms*, *30*(8), 985–1006. https://doi.org/10.1002/esp.1258

Swain, D. L. (2021). A shorter, sharper rainy season amplifies California wildfire risk. *Geophysical Research Letters*, *48*(5), e2021GL092843. https://doi.org/10.1029/2021GL092843

Swain, D. L., Langenbrunner, B., Neelin, J. D., & Hall, A. (2018). Increasing precipitation volatility in twenty-first-century California. *Nature Climate Change*, *8*(5), 427–433. https://doi.org/10.1038/s41558-018-0140-y

Synolakis, C. E., & Karagiannis, G. M. (2024). Wildfire risk management in the era of climate change. *Proceedings of the National Academy of Sciences of the United States of America Nexus*, *3*(5), pgae151. https://doi.org/10.1093/pnasnexus/pgae151

Tang, H., McGuire, L. A., Rengers, F. K., Kean, J. W., Staley, D. M., & Smith, J. B. (2019). Evolution of debris-flow initiation mechanisms and sediment sources during a sequence of postwildfire rainstorms. *Journal of Geophysical Research: Earth Surface*, *124*(6), 1572–1595. https://doi.org/10.1029/2018JF004837

Thomas, M. A., Kean, J. W., McCoy, S. W., Lindsay, D. N., Kostelnik, J., Cavagnaro, D. B., et al. (2023). Postfire hydrologic response along the central California (USA) coast: Insights for the emergency assessment of postfire debris-flow hazards. *Landslides*, *20*(11), 2421–2436. https://doi.org/10.1007/s10346-023-02106-7

Thomas, M. A., Michaelis, A. C., Oakley, N. S., Kean, J. W., Gensini, V. A., & Ashley, W. S. (2024). Rainfall intensification amplifies exposure of American Southwest to conditions that trigger postfire debris flows. *NPJ Natural Hazards*, *1*, 14. https://doi.org/10.1038/s44304-024-00017-8

Thorne, J. H., Wraithwall, J., & Franco, G. (2018). *California's changing climate 2018*. California's Fourth Climate Change Assessment, California Natural Resources Agency. Retrieved from https://www.climateassessment.ca.gov/

Thurston, L. L., Schiefer, E., McKay, N. P., & Kaufman, D. S. (2023). Suspended sediment deposition and sediment yields at Lake Peters, northeast Brooks Range, Alaska: Fluvial and lake-based approaches. *Earth Surface Processes and Landforms*, *48*(13), 2521–2535. https://doi.org/10.1002/esp.5642

Trenberth, K. E. (2011). Changes in precipitation with climate change. *Climate Research*, *47*(1), 123–138. https://doi.org/10.3354/cr00953

Turco, M., Abatzoglou, J. T., Herrera, S., Zhuang, Y., Jerez, S., Lucas, D. D., et al. (2023). Anthropogenic climate change impacts exacerbate summer forest fires in California. *Proceedings of the National Academy of Sciences of the United States of America*, *120*(25), e2213815120. https://doi.org/10.1073/pnas.2213815120

Turco, M., Jerez, S., Augusto, S., Tarin-Carrasco, P., Ratola, N., Jimenez-Guerrero, P., & Trigo, R. M. (2019). Climate drivers of the 2017 devastating fires in Portugal. *Scientific Reports*, *9*(1), 13886. https://doi.org/10.1038/s41598-019-50281-2

U.S. Geological Survey. (2024a). Streamflow records for gaging station 11439500, South Fork American River near Kyburz, California. https://doi.org/10.5066/F7P55KJN

U.S. Geological Survey. (2024b). Caldor fire, in webpage Emergency Assessment of Post-Fire Debris-Flow Hazards. Retrieved from https://landslides.usgs.gov/hazards/postfire_debrisflow/detail.php?objectid=382

U.S. Global Change Research Program. (2023). In A. R. Crimmins, C. W. Avery, D. R. Easterling, K. E. Kunkel, B. C. Stewart, et al. (Eds.), *Fifth National Climate Assessment*. U.S. Global Change Research Program. https://doi.org/10.7930/NCA5.2023.CH1

Vieira, D. C. S., Borrelli, P., Jahanianfard, D., Benali, A., Scarpa, S., & Panagos, P. (2023). Wildfires in Europe: Burned soils require attention. *Environmental Research*, *217*, 114936. https://doi.org/10.1016/j.envres.2022.114936

Vieira, D. C. S., Malvar, M. C. A., Fernandez, C. B., Serpa, D. A., & Keizer, J. J. (2016). Annual runoff and erosion in a recently burn Mediterranean forest: The effects of plowing and time since fire. *Geomorphology*, *270*, 172–183. https://doi.org/10.1016/j.geomorph.2016.06.042

Wagenbrenner, J., Coe, D., & Olsen, W. (2023). *Mitigating potential sediment delivery from post-fire salvage logging* Report No. 7 (p. 32). California Department of Forestry and Fire Protection. Retrieved from https://bof.fire.ca.gov/media/fkekcpde/3-iii-ca-forestry-report-post-fire-salvage-logging_ada.pdf

Wagenbrenner, J. W., MacDonald, L. H., Coats, R. N., Robichaud, P. R., & Brown, R. E. (2015). Effects of post-fire salvage logging and a skid trail treatment on ground cover, soils, and sediment production in the interior western United States. *Forest Ecology and Management*, *335*, 176–193. https://doi.org/10.1016/j.foreco.2014.09.016

Wagenbrenner, J. W., & Robichaud, P. R. (2014). Post-fire bedload sediment delivery across spatial scales in the interior western United States. *Earth Surface Processes and Landforms*, *39*(7), 865–876. https://doi.org/10.1002/esp.3488

23335084, 2025, 1, Downloaded from https://agupubs.onlinelibrary.wiley.com/doi/10.1029/2024EA003939, Wiley Online Library on [23/01/2025]. See the Terms and Conditions (https://onlinelibrary.wiley.com/terms-and-conditions) on Wiley Online Library for rules of use; OA articles are governed by the applicable Creative Commons License

Wagenbrenner, J. W., Robichaud, P. R., & Brown, R. E. (2016). Rill erosion in burned and salvage logged western montane forests: Effects of logging equipment type, traffic level, and slash treatment. *Journal of Hydrology*, *541*, 889–901. https://doi.org/10.1016/j.jhydrol.2016.07.049

Wang, J. A., Randerson, J. T., Goulden, M. L., Knight, C. A., & Battles, J. J. (2022). Losses of tree cover in California driven by increasing fire disturbances and climate stress. *AGU Advances*, *3*(4), e2021AV000654. https://doi.org/10.1029/2021AV000654

Warrick, J. A., Bountry, J. A., East, A. E., Magirl, C. S., Randle, T. J., Gelfenbaum, G., et al. (2015). Large-scale dam removal on the Elwha River, Washington, USA: Souce-to-sink sediment budget and synthesis. *Geomorphology*, *246*, 729–750. https://doi.org/10.1016/j.geomorph.2015.01.010

Warrick, J. A., Hatten, J. A., Pasternack, G. B., Gray, A. B., Goñi, M. A., & Wheatcroft, R. A. (2012). The effects of wildfire on the sediment yield of a coastal California watershed. *Geological Society of America Bulletin*, *124*(7–8), 1130–1146. https://doi.org/10.1130/b30451.1

Warrick, J. A., & Rubin, D. M. (2007). Suspended-sediment rating curve response to urbanization and wildfire, Santa Ana River, California. *Journal of Geophysical Research*, *112*(F2), F02018. https://doi.org/10.1029/2006JF000662

Westerling, A. L., & Bryant, B. P. (2008). Climate change and wildfire in California. *Climatic Change*, *87*(1), S231–S249. https://doi.org/10.1007/s10584-007-9363-z

Western Forestry Leadership Coalition. (2022). The true cost of wildfire in the Western U.S. Edgewater, Colorado, Western Forestry Leadership Coalition (p. 77). Retrieved from https://www.thewflc.org/sites/default/files/TrueCostofWildfire.pdf

Western Regional Climate Center. (2018). Cooperative climatological climate summaries. Retrieved from https://wrcc.dri.edu/Climate/prism_precip_maps.php

Wicherski, W., Dethier, D. P., & Ouimet, W. B. (2017). Erosion and channel changes due to extreme flooding in the Fourmile Creek catchment, Colorado. *Geomorphology*, *294*, 87–98. https://doi.org/10.1016/j.geomorph.2017.03.030

Williams, A. P., Abatzoglou, J. T., Gershunov, A., Guzman-Morales, J., Bishop, D. A., Balch, J. K., & Lettenmaier, D. P. (2019). Observed impacts of anthropogenic climate change on wildfire in California. *Earth's Future*, *7*(8), 892–910. https://doi.org/10.1029/2019EF001210

Williams, A. P., Livneh, B., McKinnon, K. A., Hansen, W. D., Mankin, J. S., Cook, B. I., et al. (2022). Growing impact of wildfire on western US water supply. *Proceedings of the National Academy of Sciences of the United States of America*, *119*(10), e2114069119. https://doi.org/10.1073/pnas.2114069119

Williams, M., Zhang, Y., Estop-Aragonés, C., Fisher, J. P., Xenakis, G., Charman, D. J., et al. (2020). Boreal permafrost thaw amplified by fire disturbance and precipitation increases. *Environmental Research Letters*, *15*(11), 114050. https://doi.org/10.1088/1748-9326-abbeb8

Zhuang, Y., Fu, R., Santer, B. D., Dickinson, R. E., & Hall, A. (2021). Quantifying contributions of natural variability and anthropogenic forcings on increased fire weather risk over the western United States. *Proceedings of the National Academy of Sciences of the United States of America*, *118*(45), e2111875118. https://doi.org/10.1073/pnas.2111875118

23335084, 2025, 1, Downloaded from https://agupubs.onlinelibrary.wiley.com/doi/10.1029/2024EA003939, Wiley Online Library on [23/01/2025]. See the Terms and Conditions (https://onlinelibrary.wiley.com/terms-and-conditions) on Wiley Online Library for rules of use; OA articles are governed by the applicable Creative Commons License